NASA CR-134795

MULTIPLE JET STUDY DATA CORRELATIONS

by

R. E. Walker and R. G. Eberhardt

AEROJET LIQUID ROCKET COMPANY
Sacramento, California 95812

Prepared for

NATIONAL AERONAUTICS AND SPACE ADMINISTRATION

NASA Lewis Research Center
Contract NAS 3-18026
J. D. Holdeman, Project Manager

1. Report No.	2. Government Accession No.	3. Recipient's Catalog No.
NASA CR-134795		

4. Title and Subtitle	5. Report Date
MULTIPLE JET STUDY DATA CORRELATIONS FINAL REPORT	April 1975 6. Performing Organization Code

7. Author(s)	8. Performing Organization Report No.
R. E. Walker and R. G. Eberhardt	10. Work Unit No.

9. Performing Organization Name and Address	11. Contract or Grant No.
Aerojet Liquid Rocket Company P. O. Box 13222 Sacramento, CA 95813	NAS 3-18026

12. Sponsoring Agency Name and Address	13. Type of Report and Period Covered
National Aeronautics and Space Administration Washington, D.C. 20546	Contractor Report 14. Sponsoring Agency Code

15. Supplementary Notes

Project Manager, James D. Holdeman, Airbreathing Engines Division, NASA Lewis Research Center, Cleveland, Ohio 44135

16. Abstract

Correlations are presented which allow determination of penetration and mixing of multiple cold air jets injected normal to a ducted subsonic heated primary air stream. Correlations were obtained over jet-to-primary stream momentum flux ratios of 6 to 60 for locations from 1 to 30 jet diameters downstream of the injection plane. Injection orifice diameters used in the correlations ranged from .64 cm to 2.54 cm and orifice spacing/diameter ratios from 2 to 6 were used. The range of geometric and operating variables makes the correlations relevant to gas turbine combustors. Correlations were obtained for the mixing efficiency between jets and primary stream using an energy exchange parameter developed on NAS 3-15703. In addition, jet centerplane velocity and temperature trajectories were correlated and centerplane dimensionless temperature distributions defined. An assumption of a Gaussian vertical temperature distribution at all stations was shown to result in a reasonable temperature field model. Data is presented which allows comparison of predicted and measured values over the range of conditions specified above.

17. Key Words (Suggested by Author(s))	18. Distribution Statement
Jet Mixing; Jet Penetration; Jets in Crossflow; Combustor Temperature Distribution; Combustion Gas Dilution	Unclassified - unlimited

19. Security Classif. (of this report)	20. Security Classif. (of this page)	21. No. of Pages	22. Price*
Unclassified	Unclassified		$3.00

* For sale by the National Technical Information Service, Springfield, Virginia 22151

TABLE OF CONTENTS

TABLE LIST

FIGURE LIST

Figure List (cont.)

NOMENCLATURE

D	Orifice diameter
E_T	Energy exchange efficiency
H	Duct height
J	Momentum flux ratio, $(\rho V^2)_J/(\rho V^2)_\infty$
L	Vertical distance from jet centerline
S	Orifice spacing
T	Temperature
V	Velocity
W	Width
$\dot{W}$	Weight flow rate
X	X distance, axis parallel to Primary
Y	Y distance, vertical axis
Z	Z distance, lateral axis

Subscripts

c	Temperature centerline
cent	Jet centerplane (Z = 0.0)
EB	Energy balance value
i	Properties at a point
j	Jet condition
mid	Jet midplane (Z = S/2.)
min	Minimum value
v	Velocity centerline
∞	Primary stream condition
1/2	Half value or half width

Superscripts

+	Plus side of jet (far side from injection plane)
-	Minus side of jet (side near injection plane)

Greek

θ_i	Temperature difference ratio, $(T_\infty - T_i)/(T_\infty - T_J)$
θ_{EB}	Energy balance temperature difference ratio $(T_\infty - T_{EB})/(T_\infty - T_J)$
ρ	Density
Ⓗ	$(\theta_{c,cent}, \theta_{EB})/(1 - \theta_{EB})$

I SUMMARY

The purpose of this study was to correlate the experimental diluent air/primary combustor gas mixing efficiency and downstream temperature distributions obtained during the Multiple Jet Study (NAS 3-15703) to gas turbine combustor operating and design variables. The experimental data were generated by probe measurements from tests on single rows of multiple dilution orifices (diameters of .64 to 2.54 cm) injected into a low Mach number (M = .03) heated primary stream (450°K to 750°K) in a 10.2 by 30.5 cm duct. The correlations were developed using power form or exponential equations which related the various dependent temperature field variables to the independent operating and design variables.

The dependent mixing and jet penetration parameters correlated at each downstream data location were: the jet/primary stream mixing efficiency; the jet temperature and velocity trajectories downstream of the injection orifice in the jet centerplane-of-symmetry; the maximum centerplane temperature difference (which is on the temperature centerline); the jet half-width values on each side of the jet centerline in the jet centerplane-of-symmetry; and the minimum temperature difference values on each side of the centerline. When coupled with the Gaussian form assumed for the profiles, these parameters completely define the centerplane temperature distribution at any downstream location.

The development of the off-centerplane temperature distribution made use of the observed Gaussian nature of the vertical temperature distribution at all stations where the flow field was influenced by the diluent jets. The off-centerplane correlations included the ratio of temperature maximum values at the lateral planes to the maximum values in the centerplane and the ratios of jet thermal penetration in the lateral planes to the thermal penetration in the centerplane. The off-centerplane half-widths were assumed to be equal to the corresponding centerplane values. Also the ratio of the minimum to maximum temperature difference at any off-centerplane location was assumed to equal the corresponding centerplane ratio.

I Summary (cont.)

The parameters and relationships described above provided the necessary input for complete characterization of the temperature field downstream of the diluent injection plane. The range of the operating and design variables used to develop the various correlations were selected to make the correlations relevant for use in the design of a wide spectrum of combustors for gas turbine engines. Five independent variables (one operating variable and four geometric variables) were used to achieve correlation of the dependent parameters with the test data. The independent variables used in the correlations and their ranges were: jet/primary momentum flux ratio, $(\rho V^2)_{jet}/(\rho V^2)_{primary}$ (6-60); orifice spacing/jet diameter ratio, S/D_J (2.5-7.5); duct height to jet diameter ratio, H/D_J (5-20); downstream distance to jet diameter ratio, X/D_J (1.25 - 30); and lateral distance to jet spacing, Z/S (0-.5). In addition, diluent to primary flow ratios of .04 to .60 were implicit in the data but were not required to correlate the data. The correlations were based on data obtained from a matrix of five axial stations, six lateral stations and 20 vertical stations in the flow field during approximately 50 tests on eleven orifice row designs.

II INTRODUCTION

The "Program to Correlate Diluent Air/Primary Combustion Gas Mixing Parameters with Gas Turbine Operating and Design Variables", was conducted under NASA Lewis Research Center contract NAS 3-18026. The correlations developed were based on data generated during the Multiple Jet Study (Contract NAS 3-15703, Ref. 1). A mixing efficiency parameter, termed the energy exchange efficiency (E_T), was defined during the performance of the Multiple Jet Study and was shown to quantify the diluent/primary stream mixing efficiencies over a range of test and operating conditions (Ref. (1)). This study extended the previous study to mathematically define the relationship between E_T and the combustor variables. Also, the study included an investigation of the correlation between the combustor variables and the temperature profiles downstream of the diluent injection plane. A goal of the program was to develop a general model which would allow predictions of flow field temperature distributions as a function of combustor operating and design variables.

Correlations of the penetration and mixing of jets in a crossflow has application to many problems of current interest, such as:

(1) Cooling of primary combustion gases with diluent air in gas turbine combustors.

(2) Cooling of hot gas streams in numerous industrial and military devices.

(3) Film Cooling of combustion chamber walls, turbine blades, and reentry vehicle nose cones.

(4) The aerodynamics of STOL and VTOL aircraft.

(5) The concentration and paths of pollutants downstream of industrial chimneys or downstream from discharge lines leading into rivers or streams.

The results of this study apply most directly to Items (1) and (2) above. The development of valid correlations for the mixing process between cool multiple jets and a hot primary gas stream has two principal interrelated benefits: (1) through proper design of secondary air admission ports, the combustor weight is reduced and packaging is improved since lengths required to achieve uniform temperature and mass flux profiles can be minimized, and (2) the decreased combustor length required for complete mixing will result in minimum residence time for production of nitrogen oxides.

Although the interaction of subsonic circular and noncircular jets injected normally into a subsonic mainstream flow has been the subject of numerous analytical and experimental studies, (Ref. 2-7), most published works to date have dealt with single jets rather than multiple jets in a bounded cross flow as required to simulate the gas turbine combustor secondary air admission problem. Two recent experimental studies, the above mentioned work done by Aerojet Liquid Rocket Company (Ref. 1) and work done by Case Western Reserve University (Ref. 8), have produced data for the study of the interaction of a row of multiple jets in a confined crossflow. Correlation

of a portion of the Reference 1 data has been done by Cox at Pratt & Whitney Aircraft (Ref. 9 and 10). The present study is based on a larger body of data than the Reference 9 study and the correlations were derived over a wider range of variables.

The correlations presented here were developed by relating the various dependent temperature field variables to the independent operating and design variables using power form or exponential equations. The basic forms of the correlating equations were developed from theoretical considerations and from observations of the empirical behavior, with the specific coefficients and exponents derived from a covariance analysis of the test data. This technique has led to correlations which are simple to apply and lead to an insight into the physical processes occurring during penetration and mixing of multiple jets in a confined crossflow.

III TECHNICAL DISCUSSION

A. Data Sample and Method of Analysis

The multiple jet correlations are based on data obtained during the performance of Contract NAS 3-15703 (Ref. 1). The centerplane correlation equations are based on multiple covariance analyses using over 200 test data points from eleven orifice row configurations at an average of four test operating conditions. A summary of the test configurations and operating conditions is contained in Table I. For the off centerplane evaluation, data from over 800 test data points was used. Although the correlations were based on the Reference 1 data, some comparisons are made with the experimental results of Reference 8. In addition, the results of the present study are compared with the results of Reference 9, which was based on selected tests from the Reference 1 data.

The covariance analyses were conducted using ALRC One-Way Multiple Covariance Analysis Program (FD 0088). The program uses standard multiple regression and covariance techniques and computational methods. The analysis may be performed for up to 20 variables and 500 groups. A trans-generation feature allows for additional variables to be generated or transformed from

the input variables as desired. For the particular requirements of the "Multiple Jet Correlation Study" the program was modified to accept input from the mass storage data files created for each dependent parameter.

Five independent variables (one operating variable and four geometric variables) were used to achieve correlation of the dependent parameters with the test data. The independent variables were: jet/primary momentum flux ratio, $(\rho V^2)_{jet}/(\rho V^2)_{primary}$; orifice spacing/jet diameter ratio, S/D^*_J; duct height to jet diameter ratio, H/D_J; downstream distance to jet diameter ratio, X/D_J; and lateral distance to jet spacing, Z/S. The diluent jet to primary stream density ratio was an additional parameter which was varied during the test series. However, over the range of density ratios tested (1.6, 2.2 and 2.7), no significant influences of the parameter were observed. Not used as a parameter to correlate the data, but implicit in the data, were diluent to primary flow ratios of .04 to .60. The correlations were based on data obtained from a matrix of five axial stations, six lateral stations and 20 vertical stations in the temperature field. The ranges of the operating and design variables used to develop the various correlations are given in Table I.

B. Correlating Parameters and Assumptions

1. Mixing Efficiency

A mixing efficiency parameter, termed the energy exchange efficiency (E_T) was defined during the performance of the Multiple Jet Study (Ref. 1) and was shown to quantify the diluent/primary stream mixing efficiency over a range of test and operating conditions (Ref. 1, 11). During the present study the E_T values were correlated as a function of the downstream distance, the combustor momentum flux ratio and the diluent jet size and spacing. The advantage of developing a correlation for a general mixing efficiency parameter, such as E_T, in addition to the other temperature field parameters, is that evaluation of this single parameter will allow the designer to quickly

---

*The orifice spacing to duct height ratio, S/H, also proved to be a valuable independent parameter, and was used in place of S/D_J in two of the correlations.

estimate the overall efficiency of the diluent/primary stream mixing process without the need to evaluate the many separate equations necessary for complete temperature field analysis.

2. Temperature Field Parameters

An illustration of the coordinate system used during the study together with a representation of the temperature field parameters is contained on Figure 1. In order to define the dimensionless temperature field downstream of the diluent injection orifices correlations must be developed for certain principal parameters and some key observations regarding the nature of the temperature field must be utilized. To develop the temperature field the diluent jet temperature trajectory in the orifice centerplane-of-symmetry downstream of the injection orifice must be defined and the temperature values along this path must be known. In addition, vertical temperature distribution shape parameters in the orifice centerplane must be defined (See Figure 1) and the shape of the temperature distribution off the centerplane must be known.

(a) Jet Trajectory Parameters

The diluent jet trajectory is defined in terms of the local penetration depth as a function of downstream distance, with both the penetration and downstream distance nondimensionalized by jet diameter. Both a velocity penetration and a thermal penetration were evaluated during this study. The velocity penetration, Y_v/D_J, is defined as the location of the maximum total pressure. The thermal penetration, Y_c/D_j, is defined as the location of the maximum temperature difference. The locus of penetration with downstream distance defines the trajectories. The thermal penetration has a direct impact on subsequent correlations for the complete temperature field.

(b) Non-Dimensional Temperature Parameters

The temperature parameter used for this study is the nondimensional temperature difference in the flow field downstream of jet injection, theta (Θ_i), defined as:

$$\theta_i = \frac{T_\infty - T_i}{T_\infty - T_J} \qquad (1)$$

where:

θ_i = Theta, nondimensional temperature difference at a point in the flow field

T_∞ = primary flow stagnation temperature

T_J = jet stagnation temperature

T_i = stagnation temperature at a point in the flow field

Theta is a measure of the temperature suppression in the flow field. The value of theta can vary from one, when measured temperature equals the jet temperature, to zero, when the measured temperature equals the primary stream temperature.

If complete mixing of the jet and mainstream flow occurs, the value of theta will be constant and T_i will be everywhere equal to the ideal equilibrium temperature between jet and mainstream. Thus,

$$\theta_{EB} = \frac{T_\infty - T_{EB}}{T_\infty - T_J} \qquad (2)$$

where:

θ_{EB} = ideal equilibrium theta

T_{EB} = stagnation temperature resulting from complete thermal energy exchange

The ideal theta is a useful parameter; a comparison between the measured local theta and the ideal theta provides a means of gauging the local mixing.

The maximum dimensionless temperature difference on the centerplane, $\theta_{c,cent}$, defines the thermal trajectory. For the case of a single jet in a semi-infinite crossflow, $1 \geq \theta_{c,cent} \geq 0$, and $\theta_{c,cent}$ is expressable as $\theta_{c,cent} \sim X^y$, Ref. 7. For multiple jets in a confined flow,

$1 \geq \theta_{c,cent} \geq \theta_{EB}$, and the power form is not appropriate. If the centerline temperature decay is expressed as,

$$\textcircled{H} = \frac{T_{EB} - T_{c,cent}}{T_{EB} - T_j} \qquad (3)$$

$\textcircled{H}$ is a measure of the flow field temperature reduction occurring along the centerline compared to the maximum possible reduction. Since $1 \geq \textcircled{H} \geq 0$, $\textcircled{H}$ can be modeled with the power form. Then $\theta_{c,cent}$ can be obtained from

$$\theta_{c,cent} = \textcircled{H} (1 - \theta_{EB}) + \theta_{EB} \qquad (4)$$

(c) Centerplane Temperature Profiles

The correlation of the thermal trajectory and the centerline maximum temperature difference are the first steps in a system of equations to define the flow field temperature distributions. The next step is the determination of the temperature profile shape factors which will allow the temperature distribution in the orifice centerplane about the jet centerline to be predicted. From the work of Holdeman (Ref. 7) and Cox (Ref. 9) and the data of Reference (1), the assumption of a Gaussian vertical temperature distribution appears to offer a simple yet accurate means of modeling the data.

Here another important difference between the single jet flow and the multiple, confined jet flow must be recognized. That is, θ does not have to decay to zero with increasing radial distance from the centerline. Thus the minimum dimensionless temperature difference above and below the centerline, $\theta^{\pm}_{min,cent}$, may be greater than zero, and must be correlated. Also, the traditional definition of the half width (the width where $\theta = \theta_{c,cent}/2$) must be modified such that $W^{\pm}_{1/2}/D_j$ is the distance from the centerline to where $\theta = (\theta_{c,cent} + \theta^{\pm}_{min,cent})/2$. This is necessary since θ may be everywhere greater than $\theta_{c,cent}/2$, and the traditional half-width would be undefined.

Using these parameters, the vertical temperature distribution in the centerplane was defined by:

$$\Delta\theta_i/\Delta\theta_c = \text{EXP}\left[-\ln 2.\left(\frac{L_i/D_J}{W^{\pm 1/2}/D_J}\right)^2\right] \quad (5)$$

where:

$\Delta\theta_i = \theta_{i,cent} - \theta^{\pm}_{min,cent}$

$\Delta\theta_c = \theta_{c,cent} - \theta^{\pm}_{min,cent}$

L_i/D_J = local distance from centerline nondimensionalized by jet diameter

$W^{\pm 1/2}/D_J$ = plus or minus side half width nondimensionalized by jet diameter

A schematic drawing of the test duct is shown on Figure 1 with a typical vertical centerplane temperature profile and temperature field parameters illustrated.

(d) Lateral Plane Temperature Profiles

Correlations for the vertical temperature distributions off the centerplane were needed in order to model the complete temperature field. These off-centerplane correlations included the ratio of the maximum temperature difference values at the lateral planes to the centerline values in the centerplane ($\theta_{c,z}/\theta_{c,cent}$) and the ratios of the jet thermal penetration in the lateral planes to the thermal penetration in the centerplane ($Y_{c,z}/Y_{c,cent}$). In addition to these correlations, the development of the off-centerplane temperature distributions made use of the observed Gaussian nature of the vertical temperature distribution at all stations where the flow field was influenced by the diluent jets. Also, the observation that the ratios of the minimum to maximum temperature difference at any off-centerplane location were essentially equal to the corresponding centerplane ratios was a key modeling relationship used in defining the complete temperature field. Another major simplifying assumption, justified by the experimental data, was that the off-centerplane half-widths were equal to the corresponding centerplane half-widths.

The parameters and relationships described in the preceding paragraphs provided the necessary input for complete characterization of the temperature field downstream of the diluent injection plane. The correlations were developed by relating the various dependent temperature field variables to the independent operating and design variables using power form or exponential equations. The basic forms of the correlating equations were developed from theoretical considerations and from observations of the empirical behavior, with the specific coefficients and exponents derived from a covariance analysis of the test data. A summary of the correlation equations is shown in Table II.

C. Mixing and Centerplane Correlation Equations

1. Energy Exchange Efficiency

An energy exchange efficiency parameter was defined in Reference 1 by:

$$E_T = \sum_{i=1}^{n} \left[\dot{W}_{Ji} \frac{(T_i - T_J)}{T_{EB} - T_J} + \dot{W}_{\infty i} \frac{(T_i - T_\infty)}{T_{EB} - T_\infty} \right] \frac{100}{\dot{W}_T}$$

where:

$\dot{W}_{Ji}$ = local jet mass flow rate

$\dot{W}_{\infty i}$ = local primary mass flow rate

$\dot{W}_T$ = total mass flow rate

The energy exchange parameter expresses the mixing effectiveness (in percent) as the energy exchanged between the cool jets and the hot primary stream, at any axial station, compared to the energy exchanged if both streams came to thermal equilibrium.. The E_T values have been shown to quantify the diluent/primary stream mixing efficiencies over a range of test and operating conditions (Ref. 1, 11). During this study the energy exchange parameter has been correlated to the combustor operating and design variables by the following relationship:

$$E_T = 100\,[1 - e^{-a}] \tag{6A}$$

where:

$$a = .682\, J^{.41} (S/D_J)^{.44} (H/D_J)^{-1.0} (X/D_J)^{.44} \tag{6B}$$

A plot of the E_T correlation equation, which has a one sigma standard error of prediction of 5.6 is shown on Figure 2. Inspection of Equations (6A) and (6B) shows E_T to be bounded by values of 0 and 100 and shows the E_T prediction to increase with increasing momentum flux ratio, J, orifice spacing, S/D_J, and downstream distance X/D_J, and orifice size $1/(H/D_J)$. The correlation was developed over the ranges of independent variables given in Table I, but excluded those specific cases (approximately 10% of the data) where jet over penetration occurred, i.e., cases combining high momentum flux ratio with large hole size and hole spacing.

2. Jet Velocity Penetration

The correlation obtained for the jet velocity penetration, Y_v/D_J, was:

$$Y_v/D_J = .549\, J^{.12} (S/D_J)^{.23} (H/D)_J^{.57} (X/D_J)^{.18} \tag{7}$$

From the form of Equation 7 one may see that increasing momentum flux ratio, duct height/orifice diameter and/or spacing increases the trajectory path depth. The agreement between the data and the correlation is shown on Figure 3.

Approximately 86% of the data are within a ± 20% band about the prediction line. This data band is a consequence of the very uniform vertical velocity distribution shown by a large portion of the data. The uniform velocity distribution caused some random scatter in the location of the maximum velocity values, however, the covariance analysis indicated good correlation with all of the above independent variables.

Velocity penetration data was also available from the work of Kamotani and Greber (Ref. 8). These data indicate less jet velocity centerline penetration than is predicted by Equation (7), except at the highest momentum flux ratios when the data from Reference 8 shows greater penetration than does the prediction. The data from Reference 8, for tests with H/D = 8 and S/D = 2, is shown on Figure 4, along with the corresponding trajectory predictions using Equation 7. Differences in primary stream boundary layer effects and jet velocity profiles may partially account for these penetration differences shown on the figure. The jet velocity profiles from Reference 8 corresponded to fully developed pipe flow while the Reference 1 work used sharp-edged orifices and the jet velocity profiles were not fully developed. Jet velocity profile differences between pipe flow and nozzle (or orifice) flow were observed to cause approximately a 10% reduction in jet penetration for the pipe compared to the nozzle (Ref. 8). If the corrections for velocity profile and boundary layer development are made to the predictions on Figure 4 agreement between measured and predicted values is improved at the lower momentum flux levels, but is worse at J = 72. The variation of the trajectory with downstream distance appears to be correctly given by Equation (7).

For most of the data surveyed the agreement between the Reference 8 data and the predictions of Equation (7) appeared best at a momentum flux ratio of 32. For much of the Reference 8 data low momentum flux ratios (J = 8) resulted in substantially less penetration than did the data of Reference 1, upon which Equation 7 is based. At high J values the Reference 8 data shows more penetration than does that of Reference 1. Apparently the influence of momentum flux ratio on jet penetration from the two sets of data are significantly different. A log-log plot of the penetration depth as a function of momentum flux ratio is shown on Figure 5 for both the Reference 8 data and the Reference 1

data with two orifice row configurations, S/D = 2 at H/D = 8 and H/D = 12. The data is shown at a location 10 diameters downstream of the injection plane. The data from Reference 1 have a constant exponent on J while the Reference 8 data indicate an increasing exponent on J with increasing J.

3. Jet Thermal Trajectory

The correlation obtained for the jet thermal penetration, Y_c/D_J, was:

$$Y_c/D_J = .539\, J^{.25} (S/D_J)^{.14} (H/D_J)^{.38} (X/D_J)^{.17} e^{-b} \qquad (8)$$

where:

$$b = (X/H)^2 (H/S - \sqrt{J}/3.5)/11.0 \qquad (9)$$

As with the velocity trajectory, increasing momentum flux ratio, duct height/orifice diameter and/or orifice spacing all tend to increase the depth of the trajectory path. However, for the thermal trajectory an exponential modifier is used to model path recurving which occurs with under penetration at far downstream distances. A correlation for Y_c/D_J was derived by Cox in Reference 9. The Reference 9 correlation is based on a baseline data case with corrections to the baseline case obtained from polynomial (up to 4th order) curve fits on X/D_J. Comparison of the correlation equation (8) with the Reference 9 correlations showed Equation 8 matched the data slightly better than do the Reference 9 correlations. The correlations of Reference 9, due to the polynomial curve fits, are not applicable for $X/D_j \succ 21$.

The agreement between the data and correlation of Equation 8 is shown on Figure 6. As with the velocity trajectory, the thermal trajectory definition was difficult due to the uniform vertical temperature profiles of a large portion of the data. Approximately 85% of the data falls in a $\pm$ 20% band about the prediction. At the far downstream locations the data scatter is more evident than at locations near the orifice injection plane. The covariance analyses indicated significant exponents for all the specified independent variables. The validity of the trajectory equation is evidenced by the good agreement between

measured and predicted temperature profiles which will be shown in Section IIIE.

4. Jet Centerline Temperature Difference Values

The correlation obtained for the jet temperature centerline values was:

$$\theta_{c,cent} = \left[\frac{1.536\ J^{-.4}}{X/D_J^{1.15}}\right]^f (1 - \theta_{EB}) + \theta_{EB} \qquad (10)$$

where:

θ_{EB} = the ideal theta defined in Equation 2

$f = \sqrt{S/H\ /\ (1 + S/H)}$

From Equation 10 the temperature centerline values, $\theta_{c,cent}$, decrease with increasing downstream distance and momentum flux ratio and is strongly influenced by θ_{EB}. Also the influences of X/D_J and J on $\theta_{c,cent}$ are coupled to the spacing, S/H. The agreement between the measured data and the correlation Equation 10 is shown on Figure 7. The data on Figure 7 are shown plotted as the prediction value as a function of the measured value, since a single correlation curve as a function of X/D_J can not be drawn due to the variable power on X/D_J in Equation 10. Approximately 85% of the data falls in a $\pm$ 10% band about the correlation line.

Centerline temperature difference ratios were measured for heated jets injected into a cool primary stream in the work done by Kamotani and Greber in Reference 8. The rates of change of the dimensionless temperature ratio, $\theta_{c,cent}$, as a function of downstream distance for the Reference 8 data were approximately the same as that shown by the cool jets in heated primary stream data used on this program. A correlation for the jet centerline dimensionless temperature ratio based on a portion of the Reference 1 data was presented in Reference 9 as an exponential decay. The form of the Reference 9 equation differed from the more conventional power form, and the prediction appeared to diverge

from the measured data at large X/D_J, although the limits on $\theta_{c,cent}$ were well defined.

5. Plus and Minus Side Minimum Temperature Difference Values

As mentioned previously, recent studies (Ref. 1, 7, and 9) have shown the vertical temperature distribution in the orifice centerplane to be approximately Gaussian in nature. Therefore the distribution can be modeled if the location ($Y_{c,cent}/D_J$) and magnitude ($\theta_{c,cent}$) of the peak theta values are known and if the distance from the centerline to some characteristic theta values (such as a half value) on the near (-) and far (+) injection sides of the jet centerline can be defined. For the case of single jet injection the characteristic distance dimension is from the centerline to the theta half values, $\theta_{c,cent}/2$. For multiple jet injection temperature difference as low as $\theta_{c,cent}/2$ may not exist on the centerplane. Thus the half-widths, $W^{\pm}_{1/2}/D_j$, are defined as the distance from the centerline to the location where:

$$\theta^{\pm}_{1/2,cent} = (\theta_{c,cent} + \theta^{\pm}_{min,cent})/2 \qquad (11)$$

To specify the profile using this definition of the half-width, the ratio, $(\theta^{\pm}_{min,cent})/(\theta_{c,cent})$ must be known for all conditions. The form chosen for these correlations was:

$$\theta^{\pm}_{1/2,cent}/\theta_{c,cent} = 1 - .5\, e^{-c^{\pm}} \qquad (12a)$$

for $\theta^{\pm}_{1/2,cent}$, and the corresponding form for the minimum value:

$$\theta^{\pm}_{min,cent}/\theta_{c,cent} = 1 - e^{-c^{\pm}} \qquad (12b)$$

For the plus side ratio:

$$c^{+} = 0.038\, J^{1.62}\, (S/D_J)^{1.5}\, (H/D_J)^{-3.67}\, (X/D_J)^{1.1} \qquad (13)$$

This correlation results in increasing plus side minimum theta ratio values with increasing downstream distance, X/D_J, increasing momentum flux ratio, J, and increasing jet spacing, (S/D_J), and jet diameter, $(H/D_J)^{-1}$. These results are reasonable because increasing all the above mentioned parameters would increase jet penetration and thus result in a trend toward higher plus side theta minimum values.

For the minimum theta values on the minus side of the jet the correlating function, $\bar{c}$, in Equation 12 was:

$$\bar{c} = 1.57\ J^{-.3}\ (S/D_J)^{-1.4}\ (X/D_J)^{.9} \qquad (14)$$

This correlation predicts increasing minus side theta ratios with increasing downstream distance, but with decreasing momentum flux ratio and orifice spacing. The orifice size did not significantly influence the minus side minimum theta ratio. The inverse relationship between the changes in the minimum theta ratio and changes in momentum flux ratio and spacing is probably due to the fact that jet penetration increases with J and S/D_J, which would allow the jet minus side theta values to decay to lower minimum values. The agreement between the data and the predictions for the plus and minus $\theta_{1/2,cent}$ values are shown on Figures 8 and 9 respectively.

6. Plus and Minus Side Half Widths

As discussed in the preceding paragraph, the $\theta^{\pm}_{1/2,cent}$ values, (Eq. 11), were the dimensionless temperature parameters used to define a characteristic dimension, the half width, used in the Gaussian dimensionless temperature distribution equation (Eq. 5). The correlation for the plus side half width nondimensionalized by the jet diameter, D_J, was:

$$W^{+}_{1.2,cent}/D_J = .162\ J^{.18}\ (S/D_J)^{-.25}\ (H/D_J)^{.5}\ (X/D_J)^{.5} \qquad (15)$$

The correlation equation for the minus side half width was derived by difference from correlations of jet total half width and plus side half width. The resulting correlation was:

III Technical Discussion (cont.)

$$\bar{W}_{1/2,cent}/D_J = .2\, J^{.15} (S/D_J)^{.27} H/D_J^{.5} (X/D_J)^{.12} \qquad (16)$$

Difficulties encountered in a direct correlation of the minus side half width were probably a consequence of the very uniform minus side dimensionless temperature profiles for a large portion of the data. This made definition of the precise location of the minus side minimum theta values difficult.

The half width correlations can not, by themselves, be related to changes in the dimensionless temperature profiles since the half width values must be coupled with the corresponding minimum and centerline theta values in order to properly interpret the influences on the dimensionless temperature profiles. For example, if $\theta^{\pm}_{min,cent}$ and $\theta_{c,cent}$ are nearly equal a uniform temperature profile will result, even for very small half width values.

D. Off-Centerplane Correlations (Z Planes)

Two off-centerplane correlation equations were developed: (1) the ratio of the maximum temperature difference at the lateral (Z) planes to the centerline values in the centerplane and; (2) the ratios of the jet thermal penetration in the lateral (Z) planes to the thermal penetration in the centerplane. The observed Gaussian nature of the vertical temperature distribution, at all stations where the flow field was influenced by the diluent jets, was used to define temperature field profiles at the off centerplane locations. The data showed the ratio of theta minimum to theta centerline values at any location off the centerplane were essentially equal to the corresponding centerplane ratios. Thus the previously developed centerplane minimum theta correlations could be applied at the off centerplane locations. Also, the off centerplane half-widths were assumed to be equal to the corresponding centerplane half-widths.

1. Ratios of Maximum Theta Values in Lateral Planes to Theta Centerline Values in Centerplane, $\theta_{c,z}/\theta_{c,cent}$

The basic form of the correlating equation for the lateral plane to the centerplane theta ratio $\theta_{c,z}/\theta_{c,cent}$ was:

$$\theta_{c,z}/\theta_{c,cent} = 1 - \left[1 - \frac{\theta_{c,mid}}{\theta_{c,cent}}\right]\left(\frac{Z}{S/2}\right)^2 \qquad (17)$$

where:

Z = local distance from centerplane to plane Z

$S/2$ = distance from centerplane to midplane

This form makes use of the mid to centerplane theta ratios and the lateral position ratio, $Z/(S/2)$. Using Equation 17 the predicted theta ratios will be between 0 and 1 and the rate of change of $\theta_{c,z}$ with Z will go to zero at the centerplane. The power on Z will cause the variation of the theta ratio with lateral distance to be parabolic. A better basic form might be one which will allow the variation of the theta ratio with lateral distance to contain an inflection point and have zero slopes at both the centerplane and midplane. However, at the present time this more sophisticated modeling doesn't appear justified or necessary. The correlation equation for $\theta_{c,mid}/\theta_{c,cent}$ is:

$$\theta_{c,mid}/\theta_{c,cent} = 1 - e^{-d} \qquad (18)$$

where:

$$d = .452\, J^{.53} (S/D_J)^{-1.53} (X/D_J)^{.83} \qquad (19)$$

Thus the midplane to centerplane ratio increases with increasing momentum flux ratio and downstream distance (more jet spreading) and decreases with increasing orifice spacing. The dimensionless jet diameter, $[H/D_J]^{-1}$ did not appear to significantly influence the theta ratios.

2. Ratio of Penetration Depth in Lateral Planes to Penetration Depth on Centerplane, $Y_{c,z}/Y_{c,cent}$

The basic form of the $Y_{c,z}/Y_{c,cent}$ correlation was identical to that used for $\theta_{c,z}/\theta_{c,cent}$;

$$Y_{c,z}/Y_{c,cent} = 1 - \left[1 - \frac{Y_{c,mid}}{Y_{c,cent}}\right]\left(\frac{Z}{S/2}\right)^2 \qquad (20)$$

with

$$Y_{c,mid}/Y_{c,cent} = 1 - e^{-g} \qquad (21)$$

where:

$$g = .227\, J^{.67}\,(S/D_J)^{-1.0}\,(X/D_J)^{.54} \qquad (22)$$

The trends predicted by this correlation are similar to those predicted by the theta ratio correlation equations.

E. The Complete Temperature Field

The parameters and relationships described above provide the necessary input for complete characterization of the temperature field downstream of the diluent injection plane. A computer code, FIELD, was developed which incorporated the various equations and relationships into a temperature field model. These correlation equations were summarized in Table II. A listing of this code is contained in the Appendix along with a sample input. The predicted temperature profiles for Figures 10 through 29 were obtained using the FIELD program.

1. Dimensionless Temperature Profiles in the Centerplane

Predicted and measured dimensionless temperature profiles in the orifice centerplanes are shown on Figures 10 through 20. The test configuration matrix of orifice sizes and spacings used to develop the centerplane correlation equations are shown on Table III along with the momentum flux ratios surveyed. The specific configurations and momentum flux ratios selected for centerplane profile illustration are shown on Table IV. The centerplane profiles are shown for downstream distance to duct height ratios of .25, .50, 1.0 and 2.0, with the exception of the H/D_J = 20 case where X/H values of .125, .25, .5 and 1.0 were used.

Figure 10 contains data from a H/D_J = 10.2 and S/D_J = 3.8 orifice row configuration at a momentum flux ratio of 26.7. This configuration approximates an "average" configuration based on H/D_J and S/D_J values. Good agreement between the empirical data and the pediction may be seen at all four downstream planes.

Data obtained with H/D_J = 10 and momentum flux ratio of 26 is shown on Figures 11, 12 and 13 for orifice spacings, S/D_J, of 2.5, 5.1 and 7.7 respectively. These data show the predicted and measured increases in jet penetration as spacing is increased. Agreement is again good between the experimental data and the prediction except for the S/D_J = 7.7 case at the first two planes when the penetration depth is under predicted by approximately 10%. The data in Figures 11 and 12 were used in demonstrating the correlation method of Reference 9, and the predictions from this reference are shown for comparison.

The effect of momentum flux ratio on the predicted and measured dimensionless temperature profiles are shown by the data of Figures 14 and 15 for nominal H/D_J = 10 and S/D_J =5 at nominal momentum flux ratios of 6 and 62 respectively. The data of Figures 14 and 15, along with the J = 26 data of Figure 12 show the increase of jet penetration with momentum flux ratio.

The data from tests of the smallest orifices, H/D_J = 20, at the closest spacing, S/D_J = 2.5 is shown on Figure 16, for a nominal momentum flux ratio of 25. Both the measured and predicted data show the small penetration distances achieved at all stations. Agreement between the prediction and the measured data is very good at the three upstream stations but only fair at X/H = 1.0. Figures 17 and 18 contain data from tests using a nominal H/D_J of 15 at S/D_J values of 2.5 and 5.1, respectively, and nominal momentum flux ratios of 60. Again agreement between the empirical data and the predictions appears good at most stations and the increase in S/D_J is shown to increase jet penetration.

Comparison of the measured and predicted profiles for the largest orifice diameter tested (H/D_J = 5) is shown on Figures 19 and 20 for J = 13.3 and S/D_J = 2.5 and for J = 27.2 and S/D_J = 5, respectively. The prediction for the J = 13.3 test appears to match measured data well. For the J = 27.2 case the prediction for X/D_J = 1.3 and X/D_J = 2.5 underestimates the jet penetration.

The test conditions used to illustrate the model applicability on Figures 11, 12, 15 and 19 were also used in the study of Reference 9. The Reference 9 predictions are shown on the figures for comparison. Based on these data the centerplane predictions using the correlations from this study appear to model the empirical data as well or better than do the predictions of Reference 9. In addition, the simplicity of the correlations developed during this study allows easy computation, provides some insight as to the physical processes occurring during penetration and mixing, and will allow confident extrapolations.

2. Dimensionless Temperature Profiles in the Lateral (Z) Planes

Predicted and measured dimensionless temperature profiles in the lateral planes are shown on Figures 21 through 29. The test configuration matrix of orifice sizes and spacings used to illustrate the lateral plane profiles are shown in Table V. The lateral planes shown on the figures are for Z/S = 0.0, (centerplane), Z/S = .2, Z/S = .3, and Z/S = .5 (midplane). With the exception of Figure 28 which shows data at X/H = .25 all the profiles are shown at a downstream distance to duct height ratio of 1.0. The data shown on Figures 21, 22 and 23 are for nominal H/D_J = 10, S/D_J = 5 and nominal momentum flux ratios of 6, 27 and 62 respectively. Both the measured and predicted data show the increase in jet penetration and the increasing spreading of the jet (less profile change with Z lateral plane) as momentum flux ratio is increased.

Data from tests with a nominal H/D_J = 10 and nominal momentum flux ratio of 26.0 are shown on Figures 24 and 25 for S/D_J values of 2.5 and 7.7 respectively. Comparison of these data and the data of Figure 22 shows the increase in centerplane jet penetration, and the flattening of the temperature profiles in the Z lateral planes, with increasing orifice spacing. Good agreement between predicted and measured temperature profiles is evident on Figures 21 through 25.

Lateral plane temperature profiles for the smallest jet diameter, H/D_J = 20 and smallest spacing S/D_J = 2.5 are shown on Figure 26. These data show the flat minus side temperature distribution in both the Y and Z directions. For the plane shown, X/H = 1.0, the predicted profiles underestimate the jet penetration slightly; agreement is better at the upstream stations as may be seen from the centerplane data of Figure 16.

Predictions for operating and design conditions used in the study of Reference 9 are shown on Figures 27, 28 and 29, with the predictions from this reference (or Reference 10) shown for comparison. The data of Figure 27 are for X/H = 1, J = 57.3, H/D_J = 15 and S/D_J = 2.5. Figure 28 shows data at X/H = .25, J = 24.7, H/D_J = 15 and S/D_J = 5 and the Figure 29 data are for the largest orifice tested, H/D_J = 5, at X/H = 1.0, S/D_J = 2.5 and J = 13.3. A comparison of the predictions based on the correlations developed during this study with those of Reference 9 show somewhat closer agreement with the measured data using the techniques developed in this report.

IV CONCLUSIONS

A. Correlation Parameters

The mixing efficiency and temperature distribution downstream from a row of multiple dilution orifices can be adequately predicted as a function of downstream distance over the range surveyed on this study provided

only that three independent variables are known:

(1) The jet to primary stream momentum flux ratio, J
(2) The nondimensional diluent orifice diameter, $(H/D_J)^{-1.0}$
(3) The nondimensional diluent orifice spacing, S/D_J

This set of independent variables will allow predictions to be made for the following parameters:

(1) The mixing efficiency (energy exchange efficiency), E_T
(2) The jet velocity and temperature centerline penetration Y_v/D_J, Y_c/D_J
(3) The maximum nondimensional temperature values in the centerplane
(4) Shape factors which allow the entire temperature field to be predicted from the assumed Gaussian profile shape

B. Model Precision

The correlations developed during this study can be used over the ranges of variables given in Table I with reasonable confidence that the predictions will be within the one sigma standard error of prediction value given for each correlation in Table II. Extrapolation somewhat beyond the range of momentum flux ratios and downstream distances listed in Table I should yield reasonable predictions. However, extrapolations beyond the specified ranges of orifice size and spacing should be done with caution. That is, the correlations given will not reduce correctly to the limits of a slot jet or a single jet. Direct use of these correlations for combustor applications involves the implicit assumptions that the range of density ratios and turbulence levels surveyed during the test program of reference 1 were adequate to have allowed characterization if a significant influence existed.

REFERENCES

1. Walker, R. E., Kors, D. L., Multiple Jet Study, Final Report, June 1973, Aerojet Liquid Rocket Company, Sacramento, Calif., CR 121217 June 1973

2. Kamotani, Yasuhiro, and Greber, Isaac: Experiments on a Turbulent Jet in a Cross Flow, Report FTAS/TR-71-62, Case Western Reserve Univ. (NASA CR 72893), June 1971

3. Keffer, J. F., and Baines, W. D.: The Round Turbulent Jet in a Cross-Wind, J. Fluid Mech. Vol. 15, Pt. 4, April 1965, pp. 481-496.

4. Callagan, E. E., and Ruggeri, R. S.: Investigation of the Penetration of an Air Jet Directed Perpendicularly to an Air Stream. NASA TN 1615, 1948

5. Ramsey, J. W., and Goldstein, R. J., Interaction of a Heated Jet with a Reflecting Stream. Report HTL-TR-92, Minnesota Univ. (NASA CR 72513), April 1970

6. Ruggeri, R. S., Callahan, E. E., and Bowden, D. T., Penetration of Air Jets Issuing from Circular, Square and Elliptical Orifices Directed Perpendicularly to an Air Stream, NACA TN 2019, 1950

7. Holdeman, J. D.: Correlation for Temperature Profiles in the Plane of Symmetry Downstream of a Jet Injected Normal to a Crossflow. NASA-TND-6966

8. Kamotani, Y., and Greber, I.: Experiments on Confined Turbulent Jets in a Cross Flow:, NASA CR 2392, March 1974

9. Cox, G. B., Jr., Correlations for Predicting the Temperature Field Produced by a Single Row of Cooled Jets Injected into a Hot, Confined Crossflow, Pratt & Whitney Aircraft, presented at the 11th JANNAF Combustion Meeting, 13 September 1974

10. Cox, G. B. Jr., Multiple Jet Correlations for Gas Turbine Engine Combustor Design, Paper No. 75-GT-45, March 1975, ASME

11. Holdeman, J. D., Walker, R. E., Kors, D. L.: Mixing of Multiple Dilution Jets with a Hot Primary Airstream for Gas Turbine Combustors, Paper 73-1249, AIAA; AIAA/SAE 9th Propulsion Conference; Las Vegas, Nevada, Nov. 1973, (NASA TMX-71426)

TABLE I

SUMMARY OF DATA RANGES

PARAMETER	NOMINAL RANGE
Momentum Flux Ratio, J	5.0 - 60.0
Flow Rate Ratio, $\dot{W}_J/\dot{W}_\infty$	.04 - .60
Density Ratio, ρ_J/ρ_∞	1.6 - 2.7
Velocity Ratio, V_J/V_∞	1.59 - 5.33
Duct Height/Jet Diameter, H/D_J	5 - 20
Jet Spacing/Jet Diameter, S/D_J	2.5 - 7.5
Jet Spacing/Duct Height, S/H	.125 - 1.0
Downstream Distance/Duct Height, X/H	.125 - 2.0
Downstream Distance/Jet Diameter, X/D_J	1.25 - 30.
Primary Stream Reynolds Number	$.3 - .8 \times 10^5$
Primary Stream Temperature	450 - 750°K
Primary Stream Velocity	15 m/sec
Jet Velocity	25 - 121 m/sec
Jet Temperature	290°K

TABLE II

SUMMARY OF CORRELATION EQUATIONS

PARAMETER	CORRELATION EQUATION	STANDARD ERROR OF PREDICTION
Energy Exchange Efficiency	$E = 100\,[\,1.0 - e^{-a}]$ $a = 0.682\,(J)^{.41}\,(S/D_J)^{.44}\,(H/D_J)^{-1.0}\,(X/D_J)^{.44}$	5.6192
Thermal Trajectory	$\frac{Y_c}{D_J} = 0.539\,(J)^{.25}\,(S/D_J)^{.14}\,(H/D_J)^{.38}\,(X/D_J)^{.17}\,e^{-b}$ $b = (X/H)^2\,(H/S - \sqrt{J}/3.5)/11.0$	0.7518
Velocity Trajectory	$\frac{Y_v}{D_J} = 0.549\,(J)^{.12}\,(S/D_J)^{.23}\,(H/D_J)^{.57}\,(X/D_J)^{.18}$	0.7735
Centerplane Temperature Difference Ratio	$\theta_c = \left[\frac{1.536\,(J)^{-.40}}{(X/D_J)^{1.15}}\right]^f (1.0 - \theta_{EB}) + \theta_{EB}$ $f = \left[\frac{(S/H)}{1 + (S/H)}\right]^{.5}$	0.0360
Plus-Side Minimum Temperature Difference Ratio	$\frac{\theta^+_{min,cent}}{\theta_{c,cent}} = [1.0 - e^{-c^+}]$ $c^+ = 0.038\,(J)^{1.62}\,(S/D_J)^{1.5}\,(H/D_J)^{-3.67}\,(X/D_J)^{1.1}$	0.1216

TABLE II (cont.)

PARAMETER	CORRELATION EQUATION	STANDARD ERROR OF PREDICTION
Minus-Side Minimum Temperature Difference Ratio	$\frac{\theta^-_{min,cent}}{\theta_{c,cent}} = [1.0 - e^{-c^-}]$ $c^- = 1.57\ (J)^{-.3}\ (S/D_J)^{-1.4}\ (X/D_J)^{.9}$	0.734
Plus Side Half Width	$\frac{W^+_{1/2,cent}}{D_J} = 0.162\ (J)^{.18}\ (S/D_J)^{-.25}\ (H/D_J)^{.5}\ (X/D_J)^{.5}$	0.6598
Minus Side Half Width	$\frac{W^+_{1/2,cent}}{D_J} = .20\ (J)^{.15}\ (S/D_J)^{.27}\ (H/D_J)^{.5}\ (X/D_J)^{.12}$	0.5503
Midplane to Centerplane Theta Ratio	$\frac{\theta_{c,mid}}{\theta_{c,cent}} = [1.0 - e^{-d}]$ $d = 0.452\ (J)^{.53}\ (S/D_J)^{-1.53}\ (X/D_J)^{.83}$	0.1120
Off-Centerplane to Centerplane Theta Ratio	$\frac{\theta_{c,z}}{\theta_{c,cent}} = 1.0 - \left[1.0 - \left(\frac{\theta_{c,mid}}{\theta_{c,cent}}\right)\right]\left[\frac{Z}{S/2}\right]^{2.0}$	0.1109
Midplane to Centerplane Penetration Ratio	$\frac{Y_{c,mid}}{Y_{c,cent}} = [1.0 - e^{-g}]$ $g = 0.227\ (J)^{.67}\ (S/D_J)^{-1.0}\ (X/D_J)^{.54}$	0.1446
Off-Centerplane to Centerplane Penetration Ratio	$\frac{Y_{c,z}}{Y_{c,cent}} = 1.0 - \left[1.0 - \left(\frac{Y_{c,mid}}{Y_{c,cent}}\right)\right]\left[\frac{Z}{S/2}\right]^{2.0}$	0.1208

TABLE III

MATRIX OF TEST CONFIGURATIONS AND MOMENTUM FLUX RATIOS USED TO DEVELOP CORRELATIONS

H/D_J	S/D_J = 2.5	3.75	5.0	7.5
5	6-39(1)	N.T(2)	6-60	N.T.
7.5	6-60	6-26(4)	N.T.	N.T.
10	6-60	6-30(5)	6-60	6-60
15	14-60(3)	N.T.	6-60	N.T.
20	6-60	N.T.	N.T.	N.T.

(1) No Tests Conducted with J Greater than 39

(2) N.T. = Not Tested

(3) J = 6 Test not Used - Invalid Thermocouple Data

(4) J = 60 Test Not Used - Stored Test Data Could Not be Recovered
Actual $S/D_j = 3.54$; $H/D_j = 7.07$

(5) No Tests Conducted with J Greater than 30

TABLE IV

MATRIX OF TEST CONFIGURATIONS AND MOMENTUM
FLUX RATIOS USED TO ILLUSTRATE CENTERPLANE DIMENSIONLESS TEMPERATURE PROFILES

	S/D_J			
	2.5	3.75	5.0	7.5
H/D_J				
5	J=13	N.T.(1)	J=27.2	N.T.
7.5	Not Used (2)	Not Used	N.T.	N.T.
10	J=25	J=25	J=6 J=26 J=60	J=25
15	J=57	N.T.	J=60	N.T.
20	J=25	N.T.	N.T.	N.T.

(1) Not Tested

(2) Tested But Not Illustrated

TABLE V

MATRIX OF TEST CONFIGURATION AND MOMENTUM FLUX RATIO
USED TO ILLUSTRATE LATERAL PLANE DIMENSIONLESS TEMPERATURE PROFILES

H/D_J	S/D_J = 2.5	3.75	5.0	7.5
5	J=13.3 X/H=1.0	(1) N.T.	Not Used	N.T.
7.5	Not (2) Used	Not Used	N.T.	N.T.
10	J=25 X/H=1.0	Not Used	J=6 J=26 J=60 X/H=1.0	J=25 X/H=1.0
15	J=57 X/H=1.0	N.T.	J=24.7 X/H=.25	N.T.
20	J=25 X/H=1.0	N.T.	N.T.	N.T.

(1) Not Tested

(2) Tested But Not Illustrated

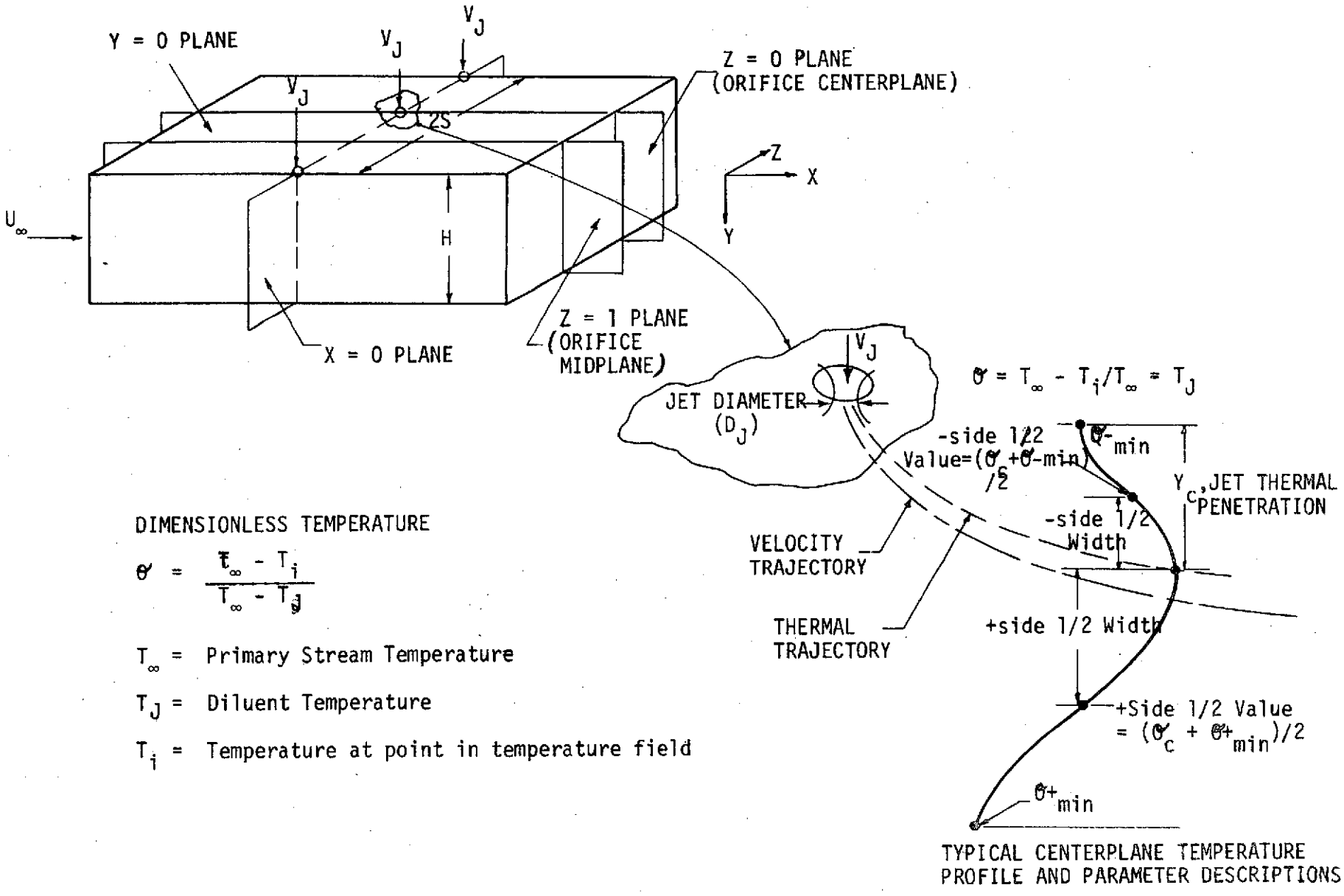

DIMENSIONLESS TEMPERATURE

$$\theta = \frac{T_\infty - T_i}{T_\infty - T_J}$$

T_∞ = Primary Stream Temperature

T_J = Diluent Temperature

T_i = Temperature at point in temperature field

FIGURE 1. MULTIPLE JET STUDY COORDINATE SYSTEM

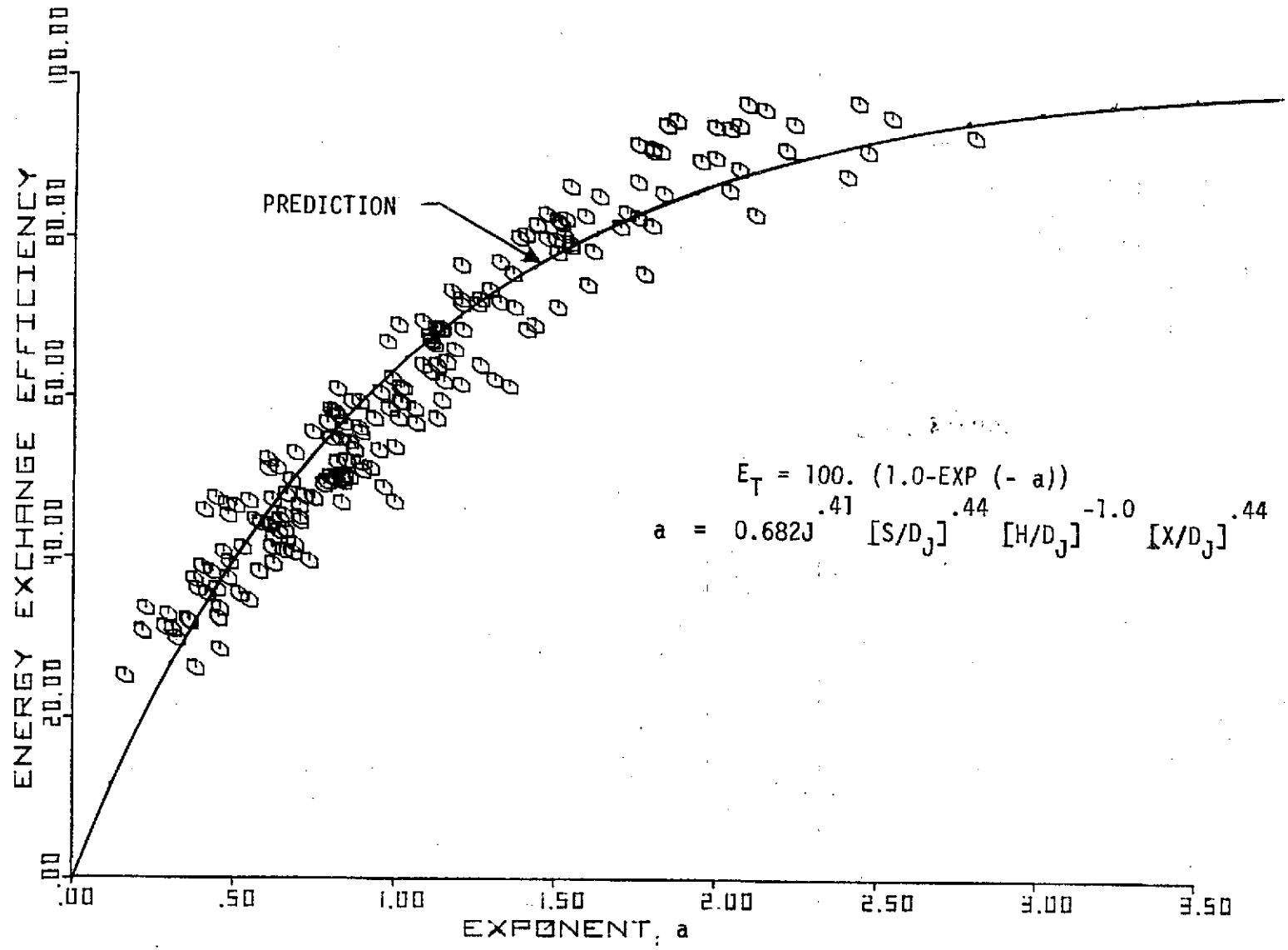

FIGURE 2. ENERGY EXCHANGE EFFICIENCY CORRELATION

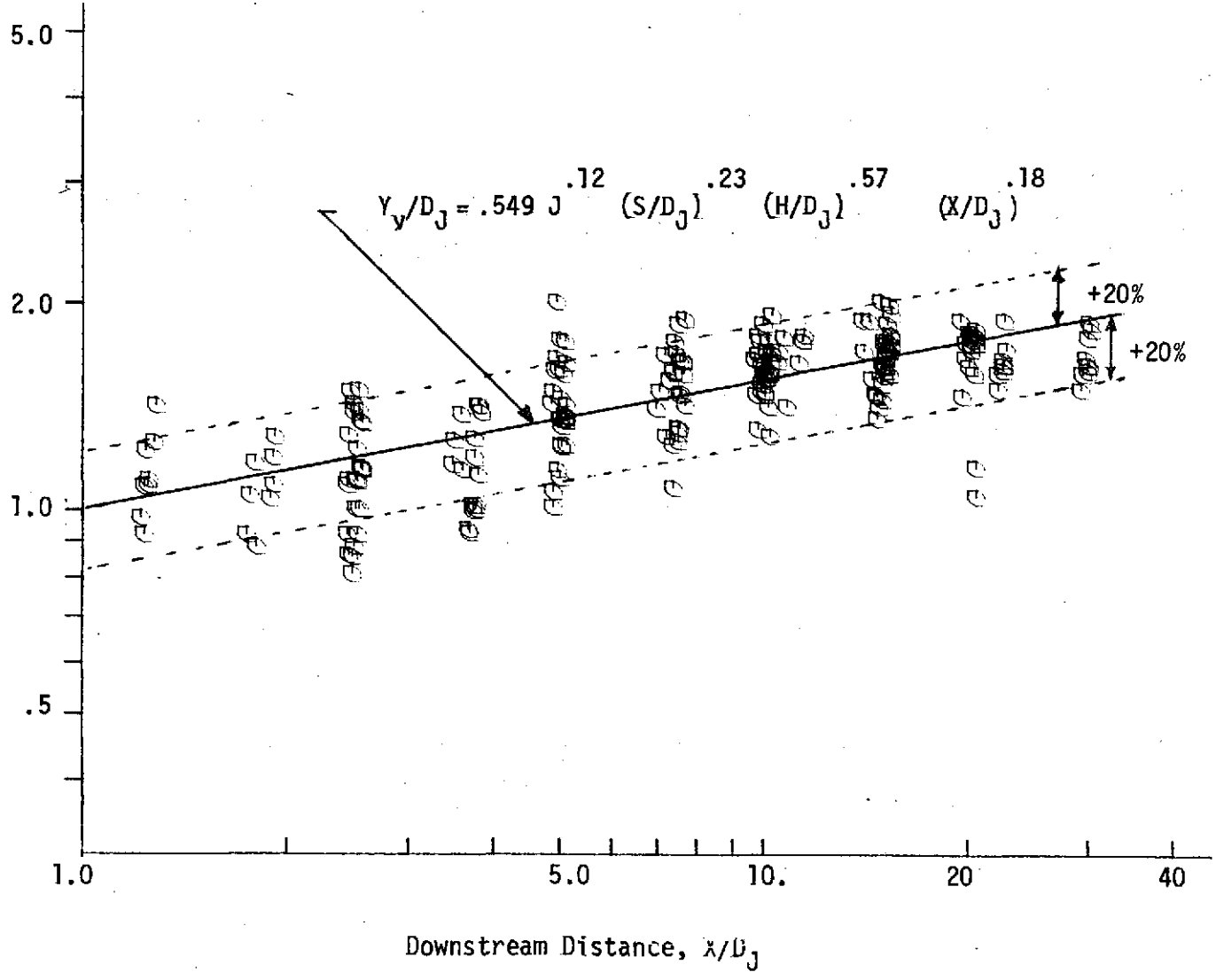

FIGURE 3. VELOCITY TRAJECTORY CORRELATION

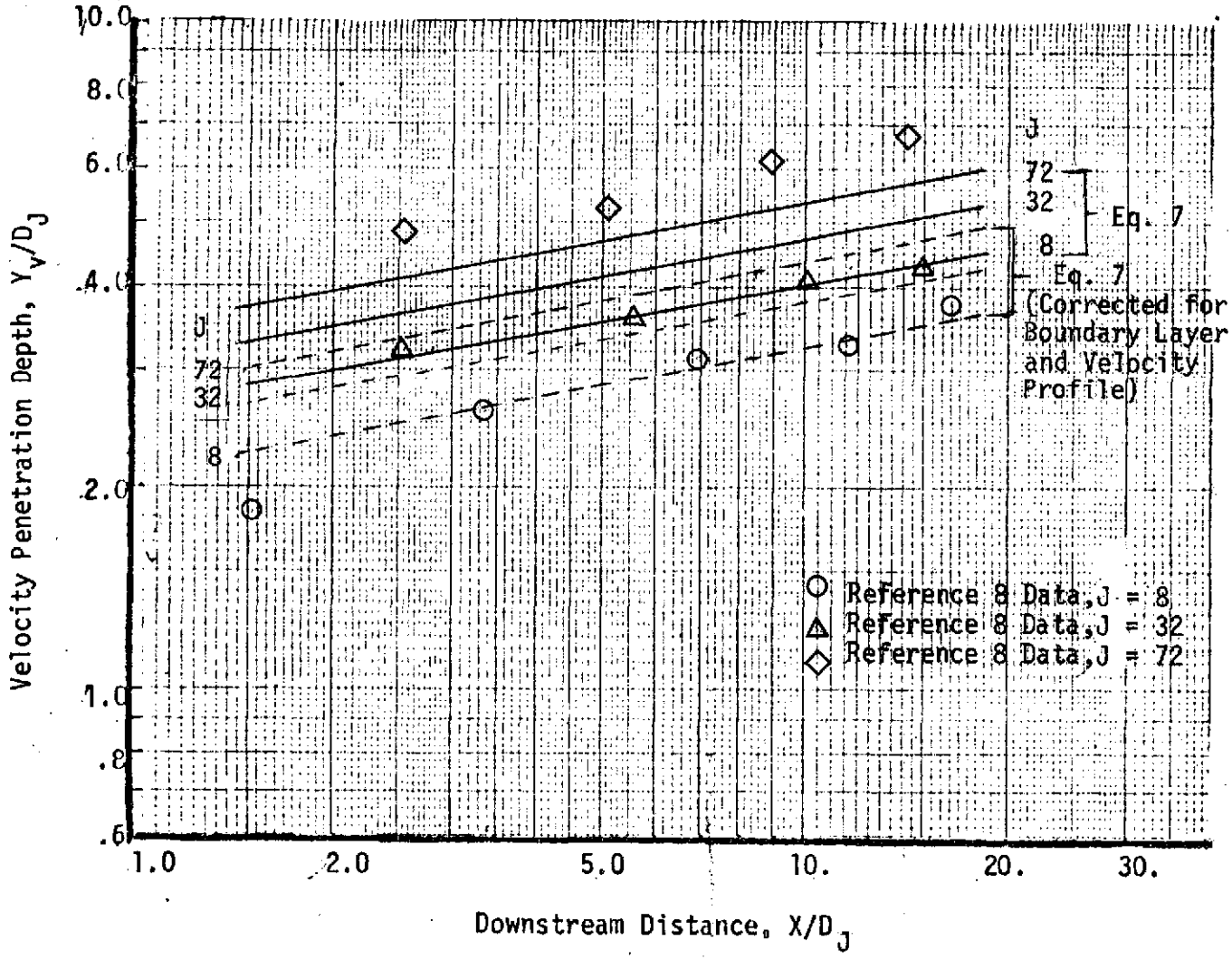

FIGURE 4. COMPARISON OF VELOCITY PENETRATION DATA H/D = 8, S/D = 2

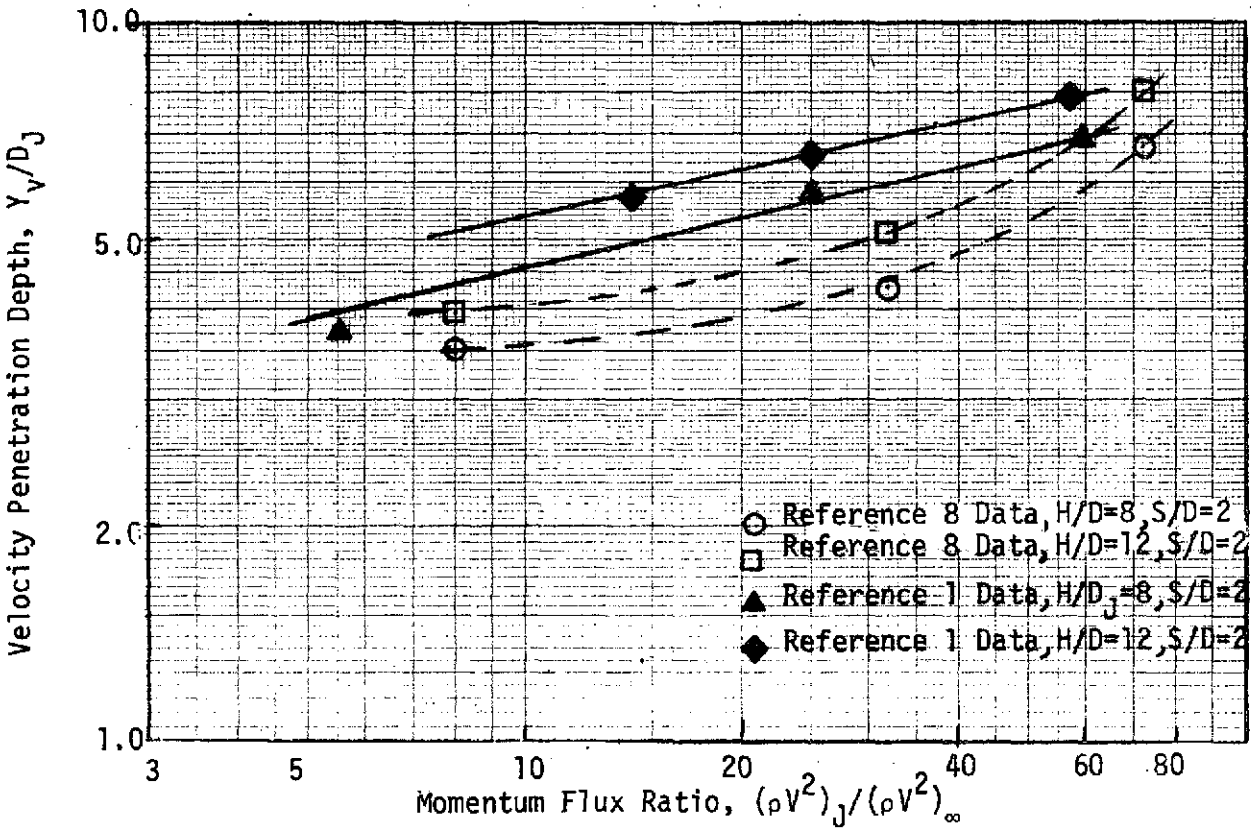

FIGURE 5. COMPARISON OF EFFECT OF MOMENTUM FLUX RATIO ON JET VELOCITY PENETRATION AT $X/D_J = 10$

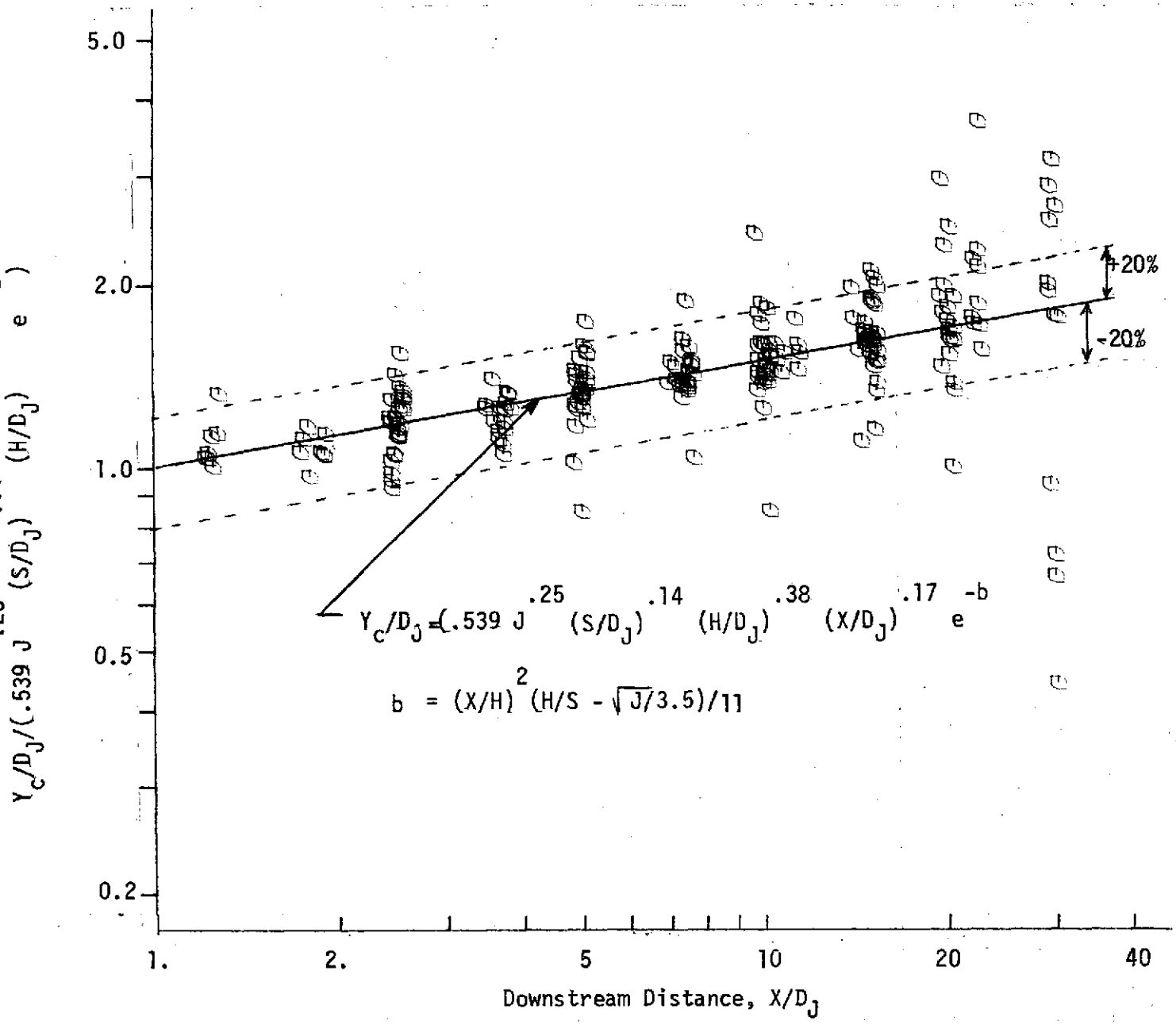

FIGURE 6. JET CENTERPLANE THETA TRAJECTORY CORRELATION

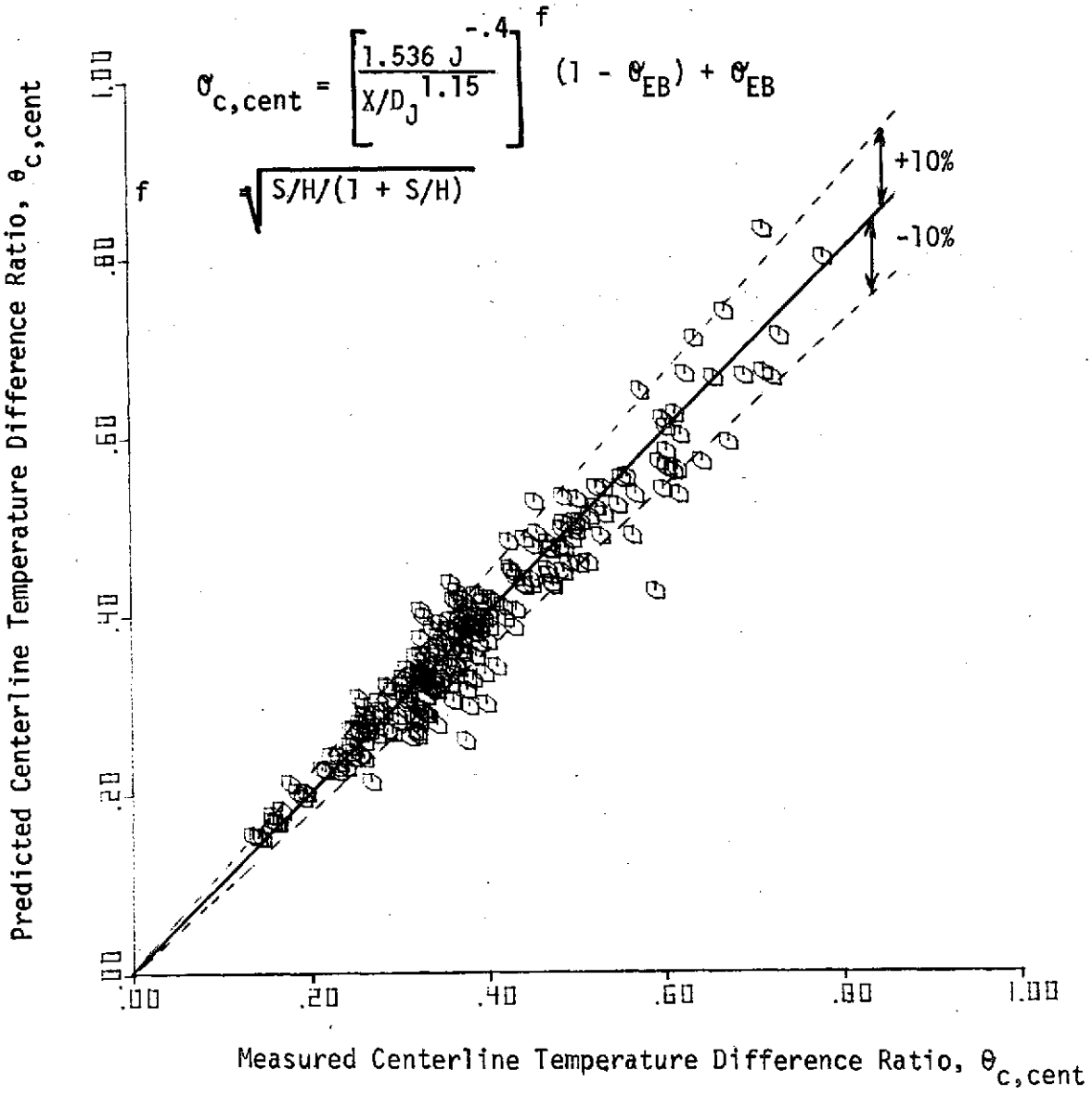

FIGURE 7. JET CENTERPLANE CENTERLINE THETA CORRELATION

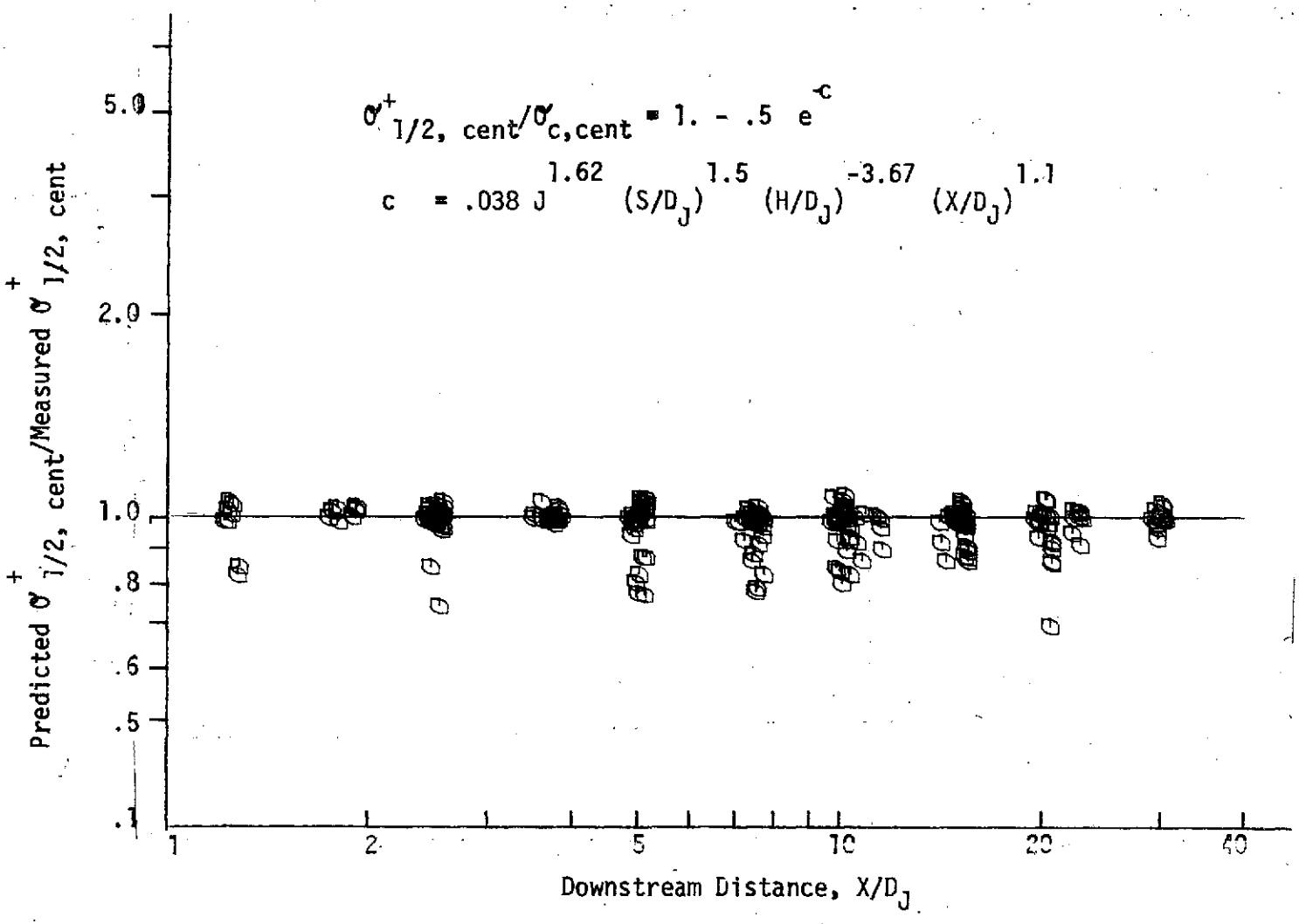

FIGURE 8. JET CENTERPLANE PLUS SIDE $\sigma^+_{1/2,cent}$ CORRELATION

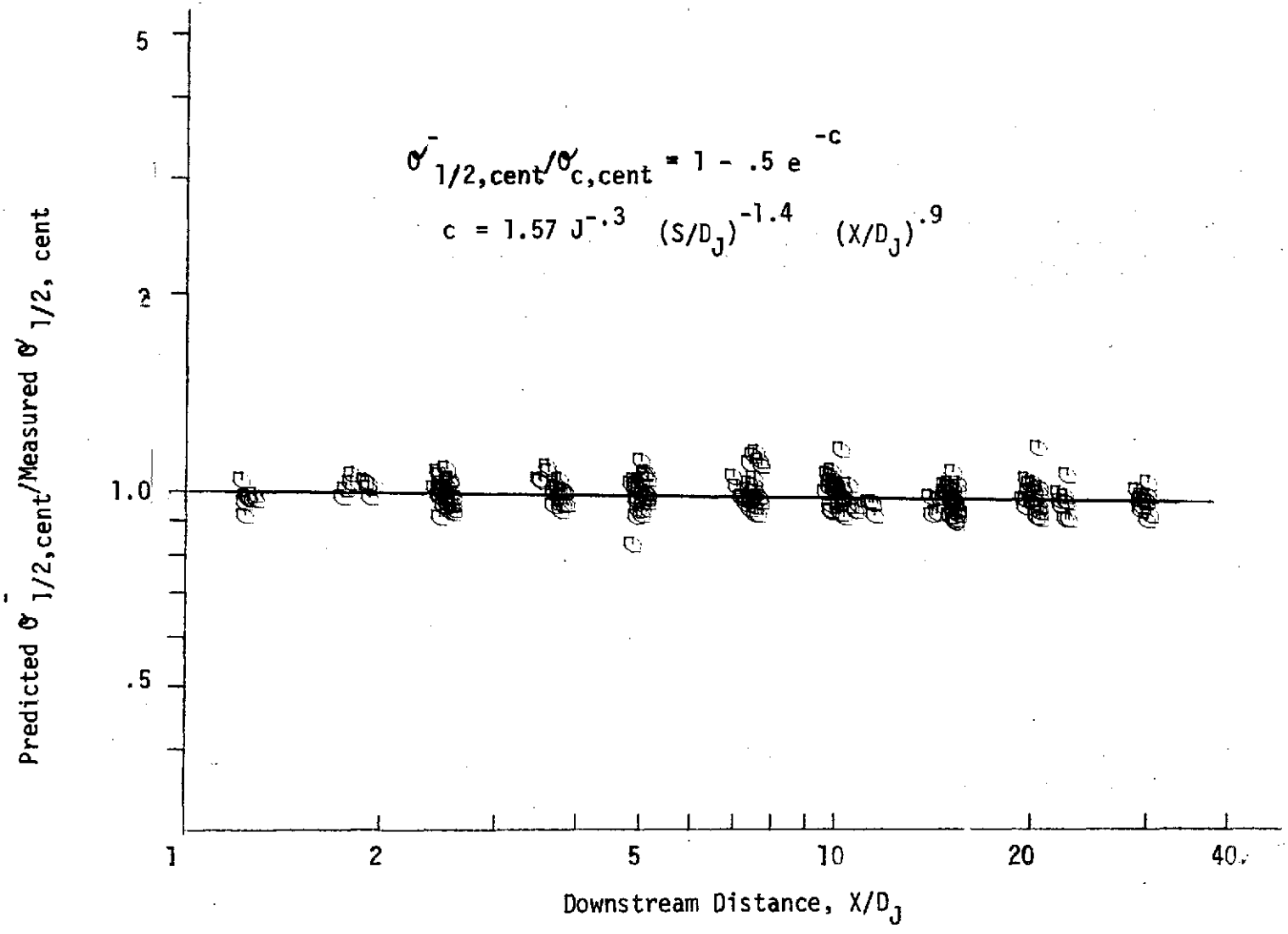

FIGURE 9. JET CENTERPLANE PLUS SIDE $\bar{\sigma}_{1/2,cent}$ CORRELATION

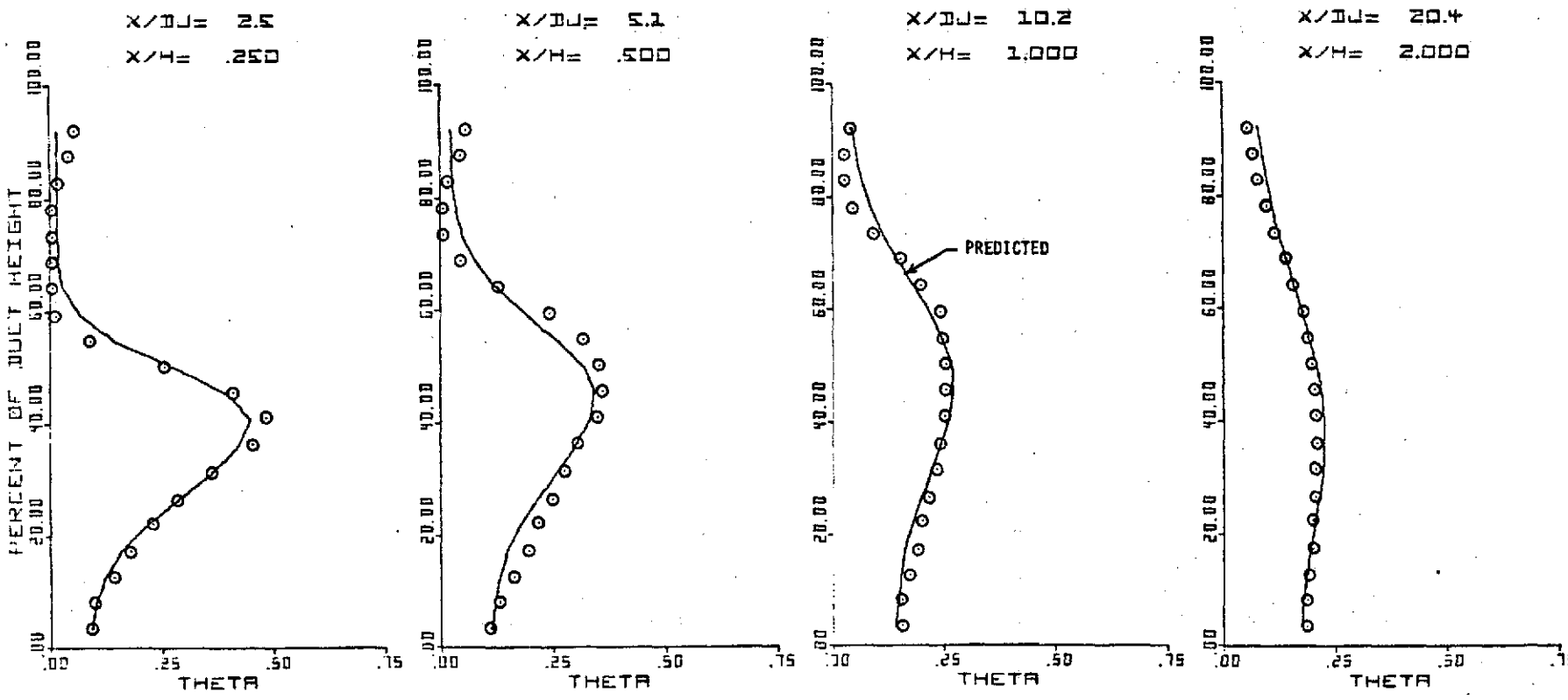

FIGURE 10. CENTERPLANE TEMPERATURE PROFILE COMPARISONS
$J = 26.7$, $S/D_J = 3.8$, $H/D_J = 10.2$

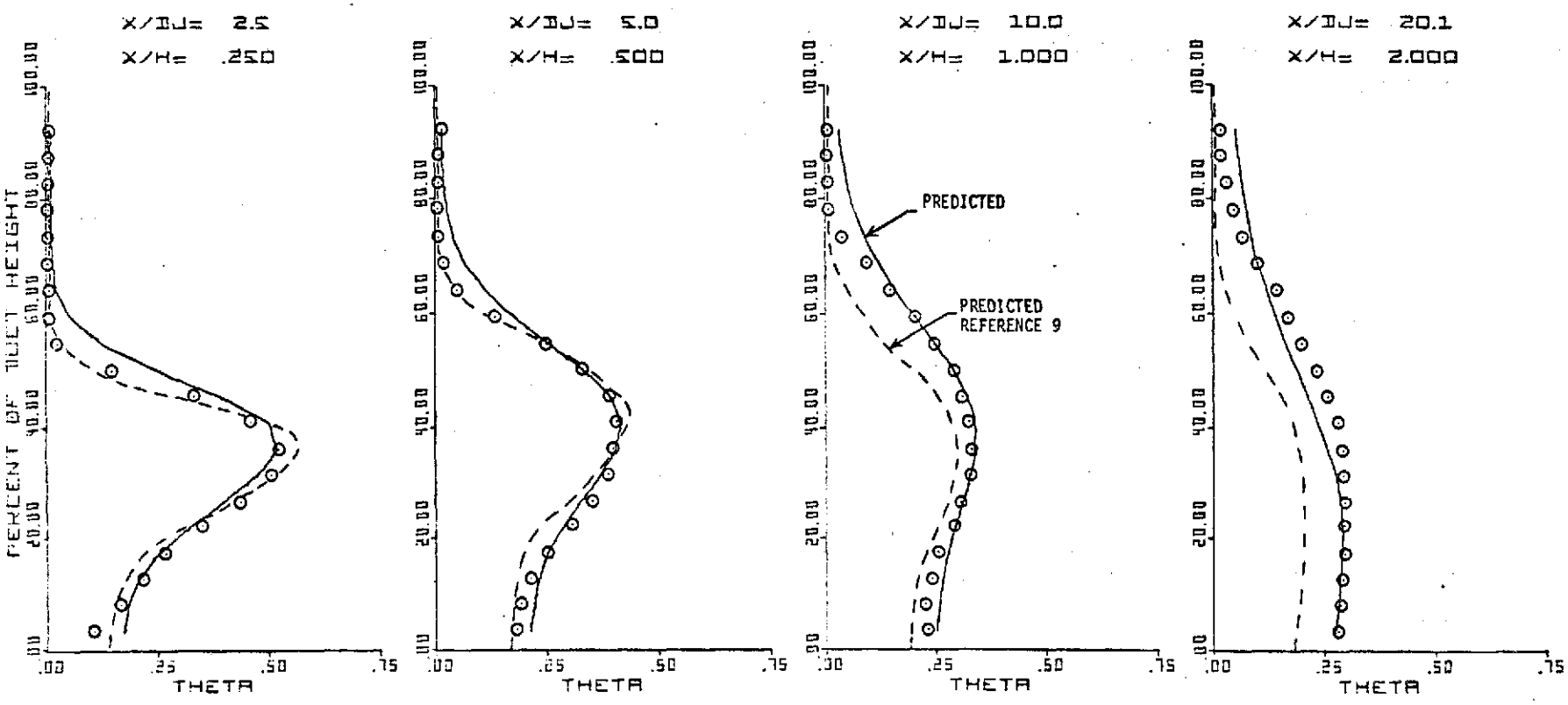

FIGURE 11. CENTERPLANE TEMPERATURE PROFILE COMPARISONS
$J = 25.2$, $S/D_J = 2.5$, $H/D_J = 10.0$

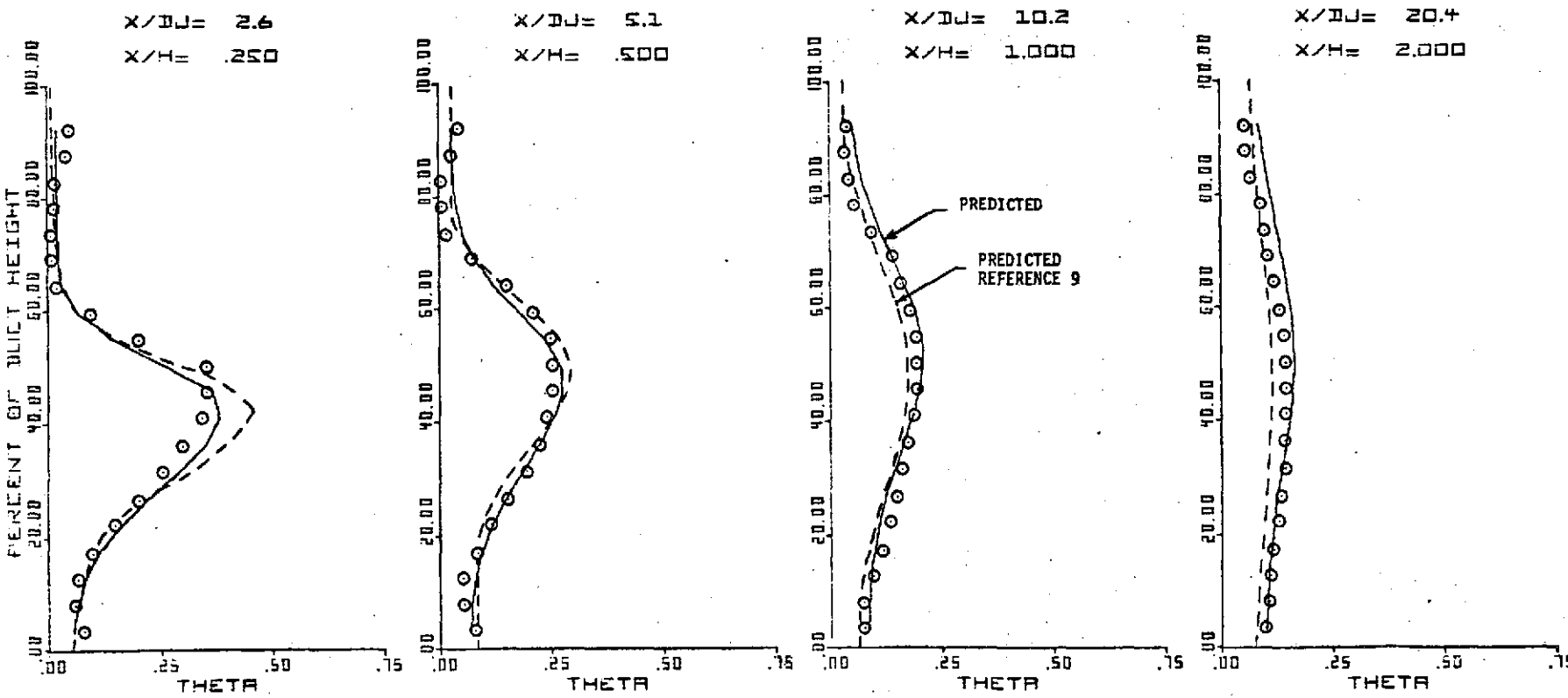

FIGURE 12. CENTERPLANE TEMPERATURE PROFILE COMPARISONS
$J = 26.8$, $S/D_J = 5.1$, $H/D_J = 10.2$

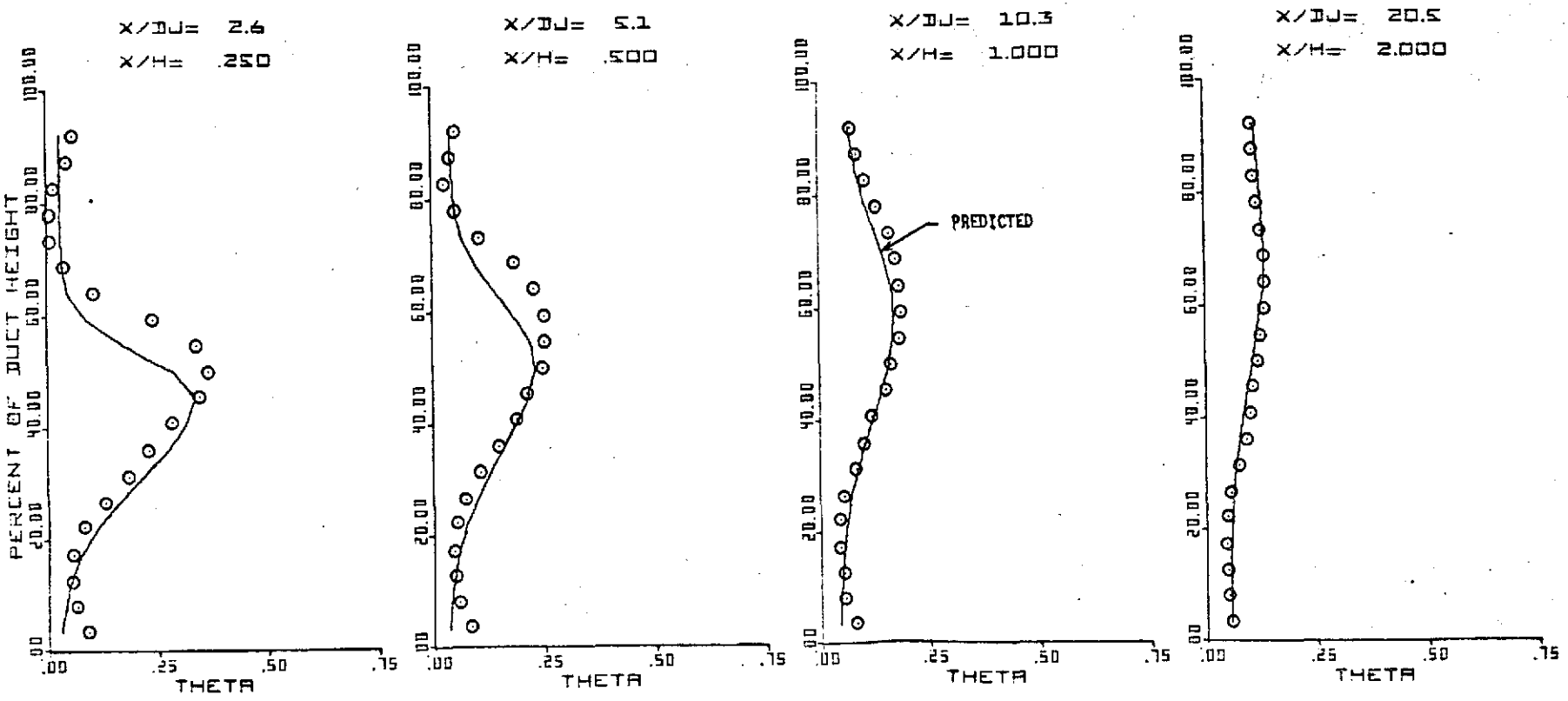

FIGURE 13. CENTERPLANE TEMPERATURE PROFILE COMPARISONS
$J = 27.6$, $S/D_J = 7.7$, $H/D_J = 10.3$

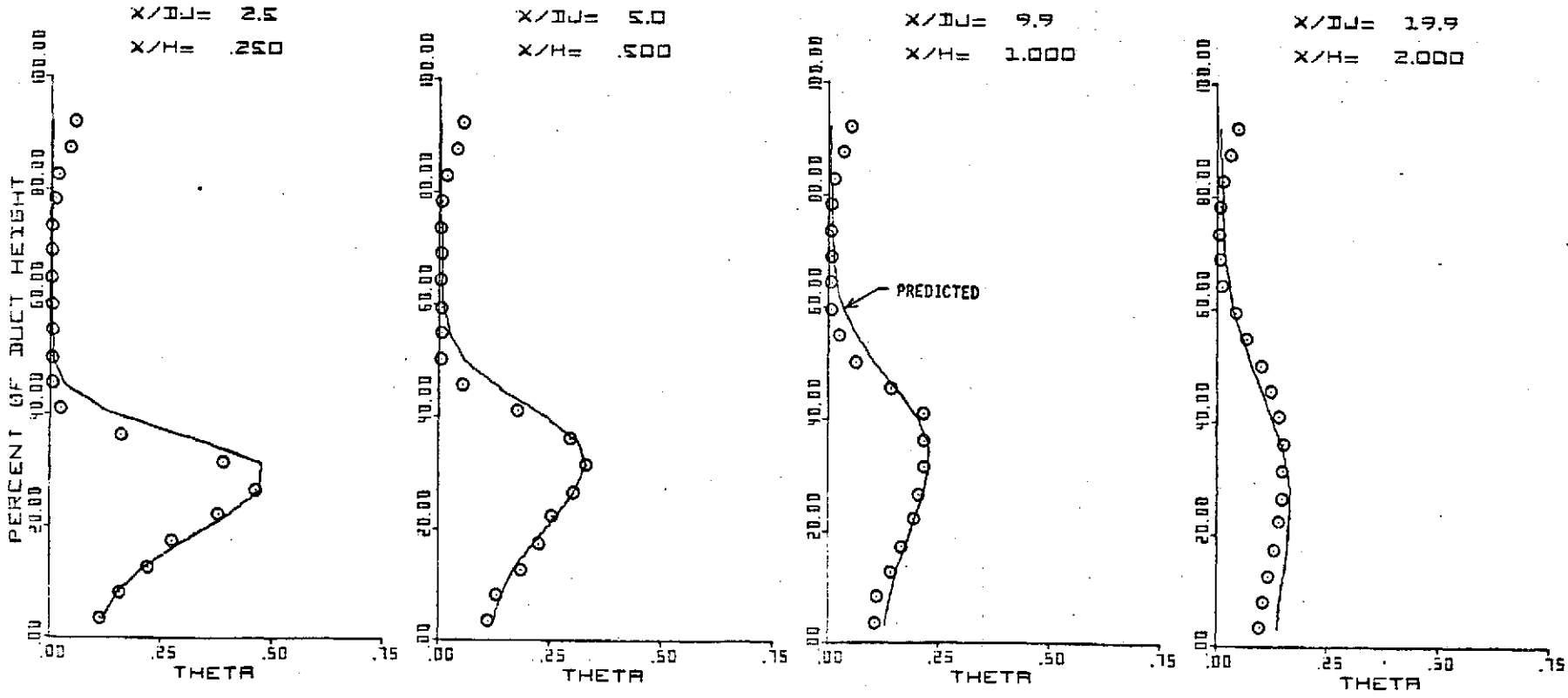

FIGURE 14. CENTERPLANE TEMPERATURE PROFILE COMPARISONS
$J = 6.3$, $S/D_J = 5.0$, $H/D_J = 9.9$

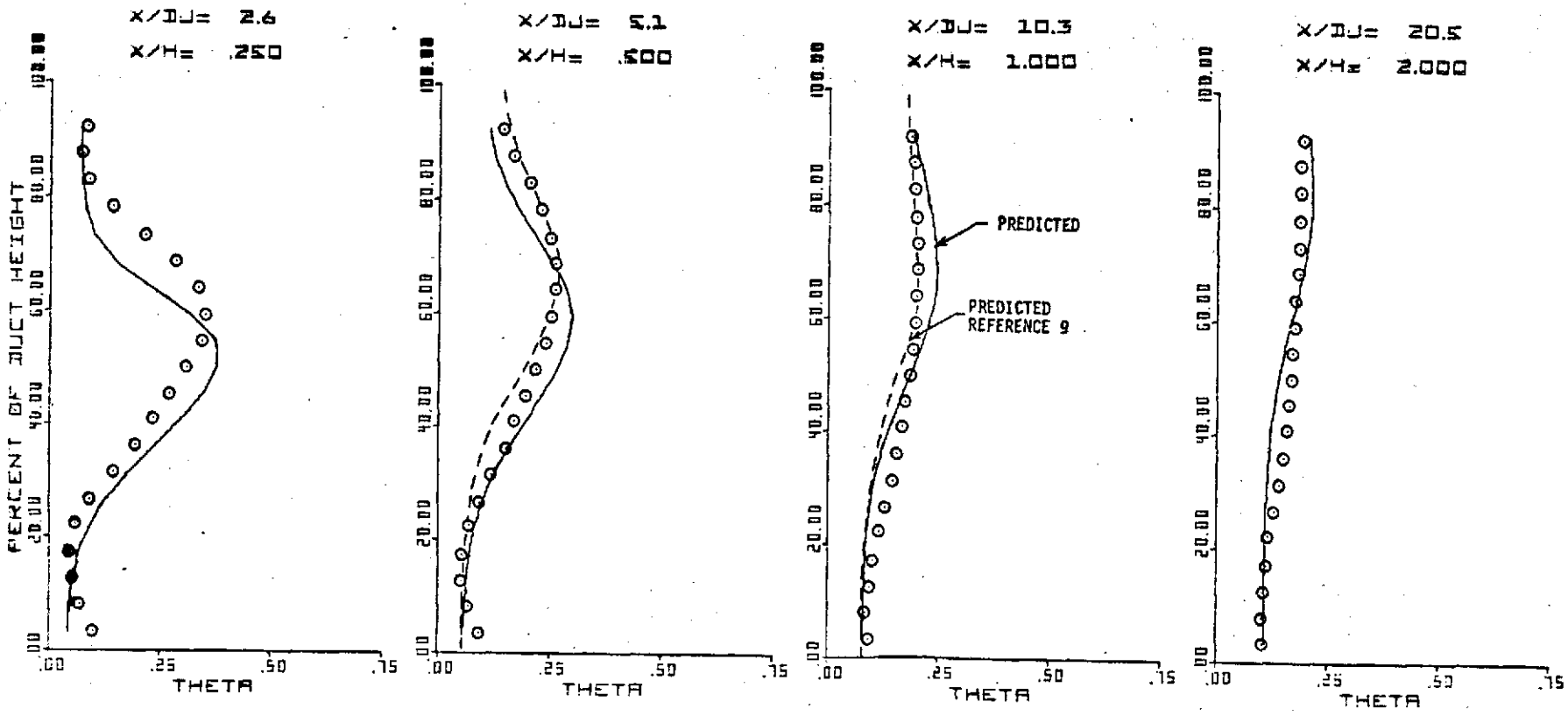

FIGURE 15. CENTERPLANE TEMPERATURE PROFILE COMPARISONS
$J = 61.9$, $S/D_J = 5.1$, $H/D_J = 10.3$

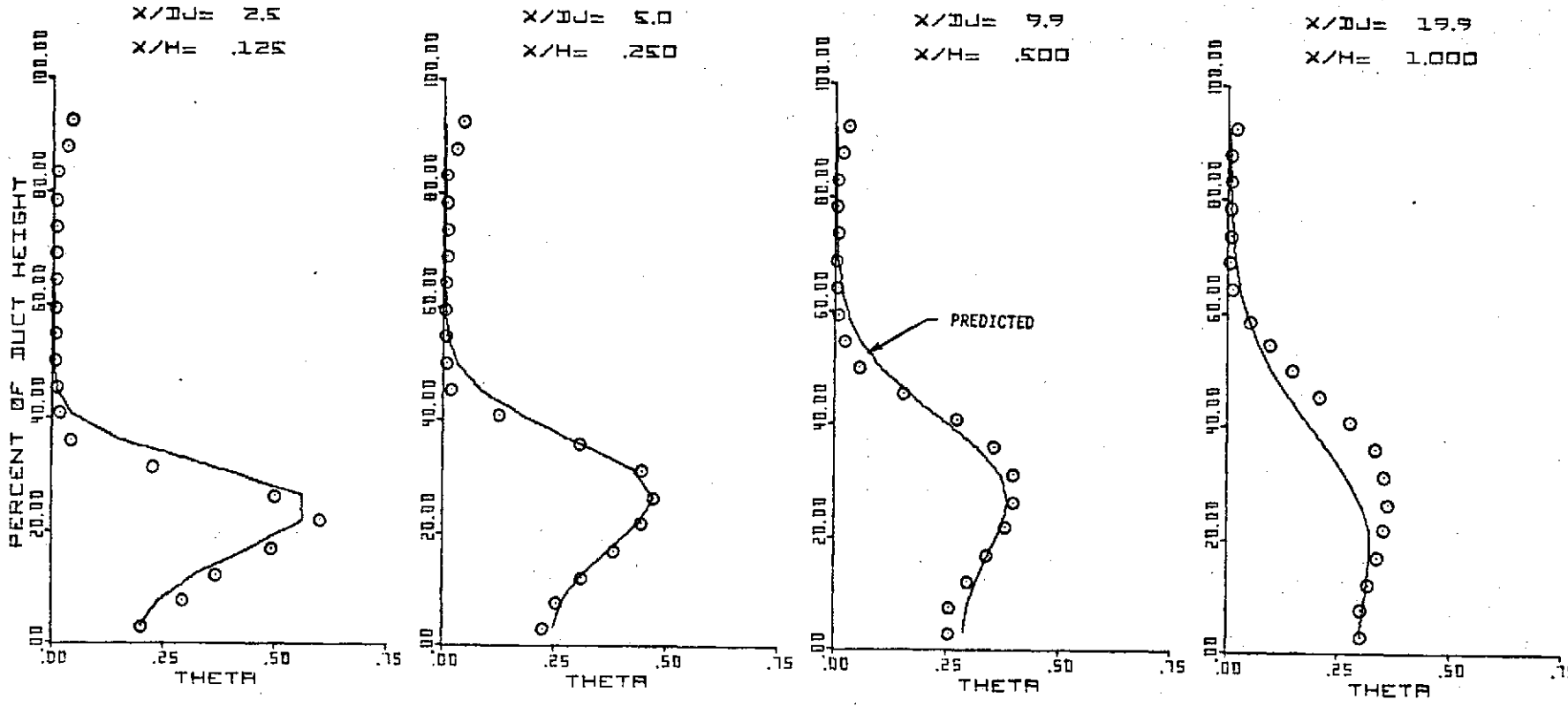

FIGURE 16. CENTERPLANE TEMPERATURE PROFILE COMPARISONS
$J = 25.0$, $S/D_J = 2.5$, $H/D_J = 19.9$

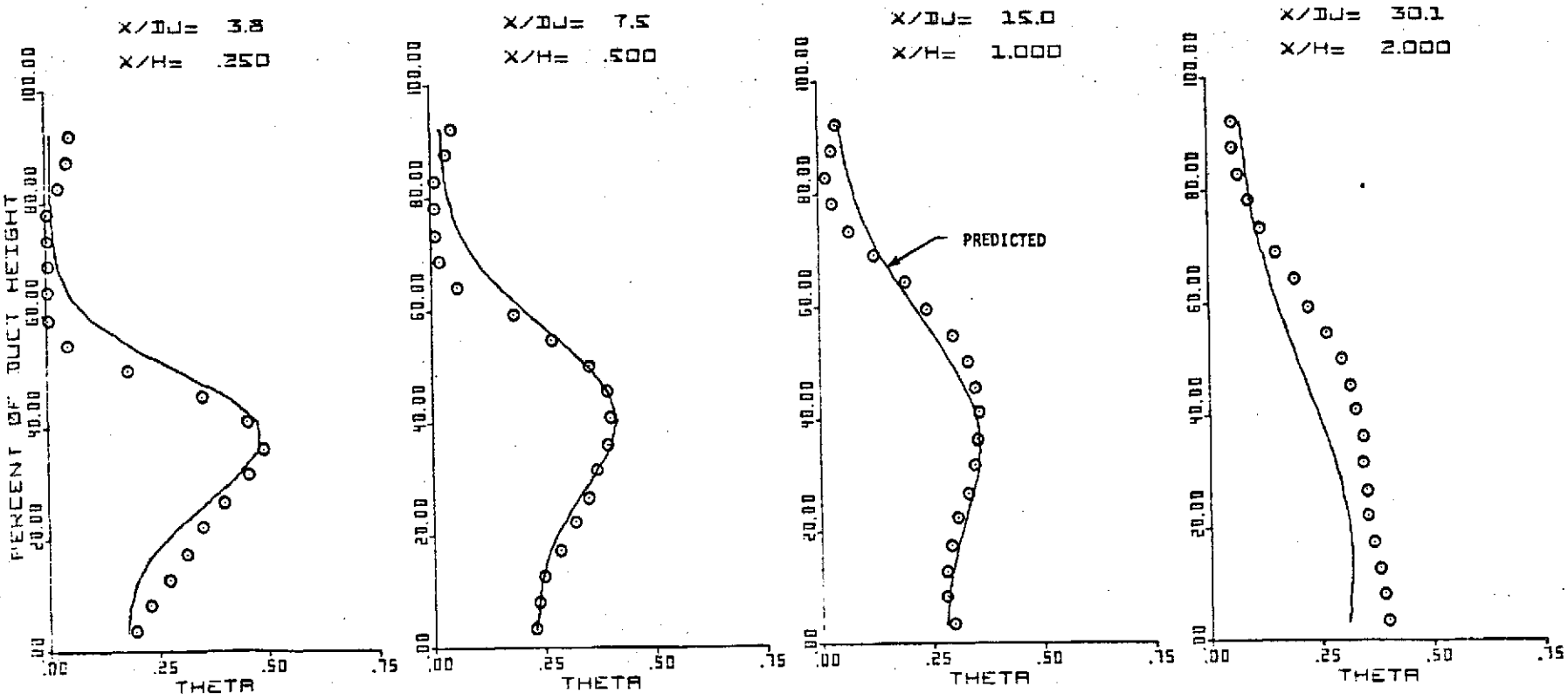

FIGURE 17. CENTERPLANE TEMPERATURE PROFILE COMPARISONS
$J = 57.3$, $S/D_J = 2.5$, $H/D_J = 15.0$

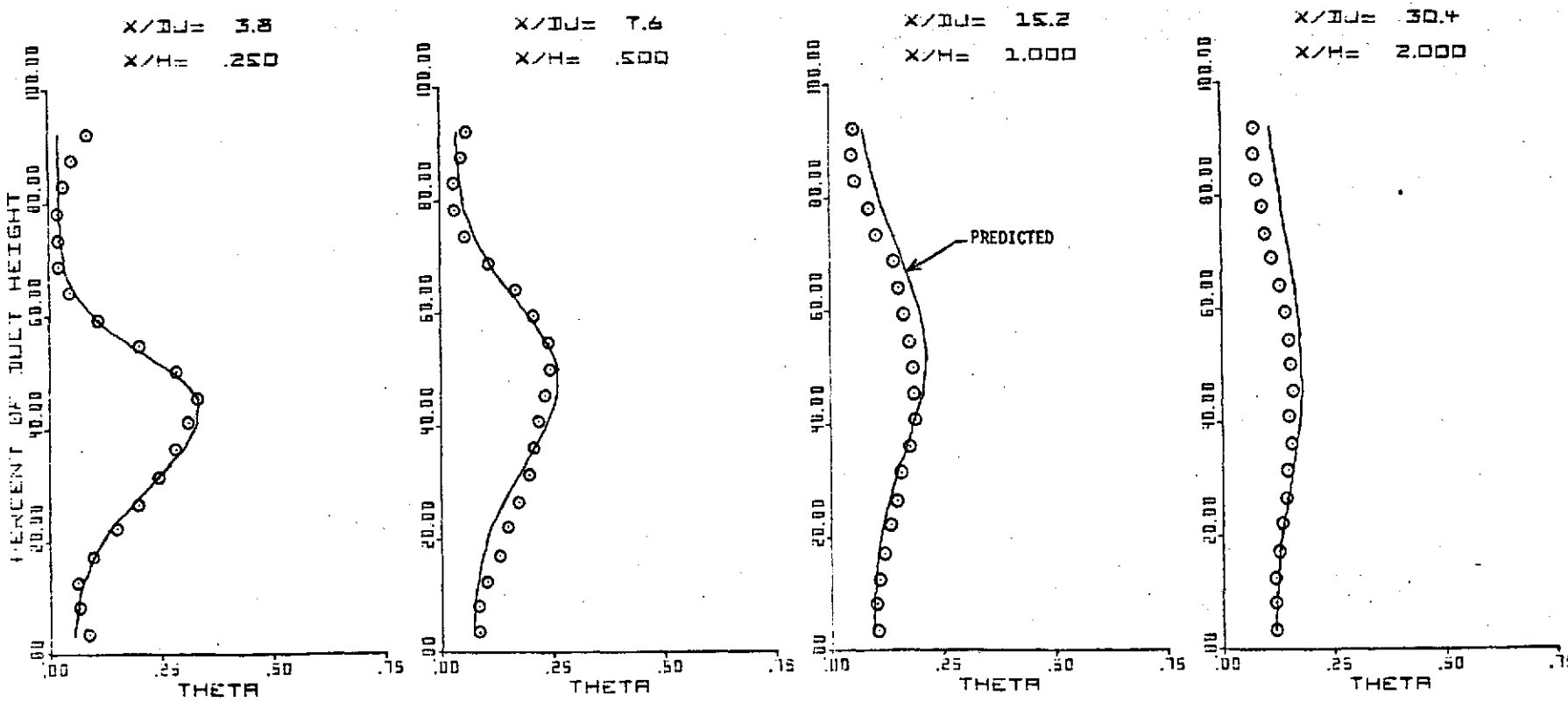

FIGURE 18. CENTERPLANE TEMPERATURE PROFILE COMPARISONS
$J = 60.3$, $S/D_J = 5.1$, $H/D_J = 15.2$

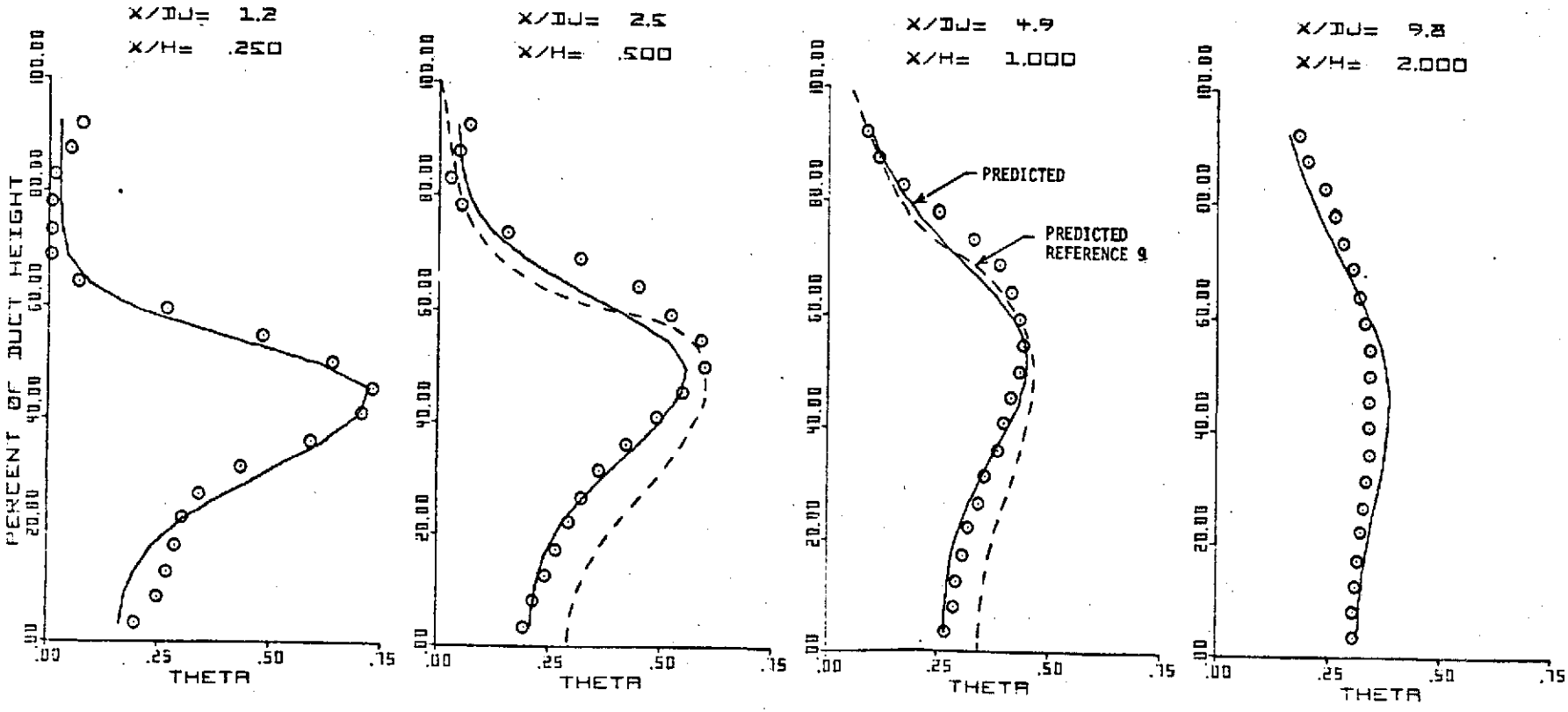

FIGURE 19. CENTERPLANE TEMPERATURE PROFILE COMPARISONS
$J = 13.3$, $S/D_J = 2.5$, $H/D_J = 4.9$

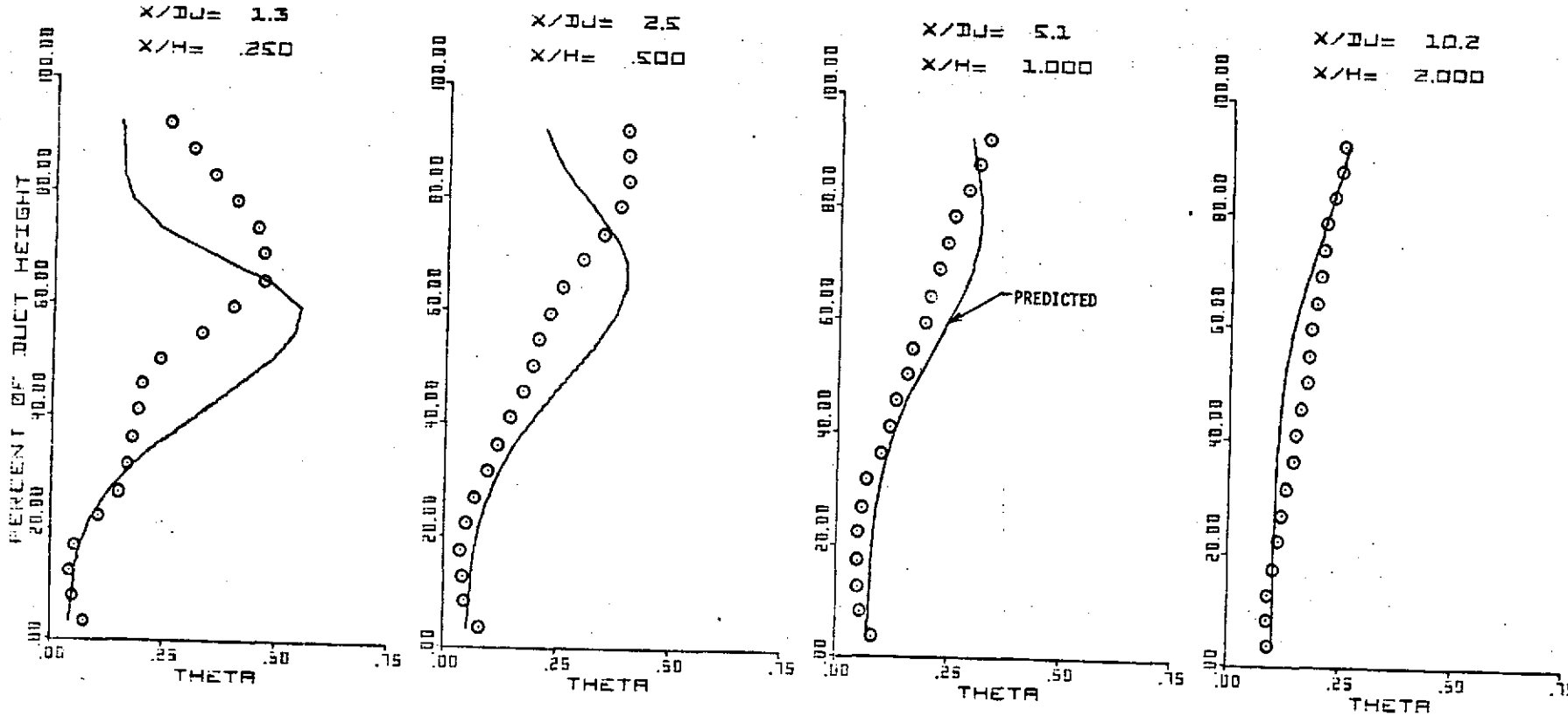

FIGURE 20. CENTERPLANE TEMPERATURE PROFILE COMPARISONS
$J = 27.2$, $S/D_J = 5.1$, $H/D_J = 5.1$

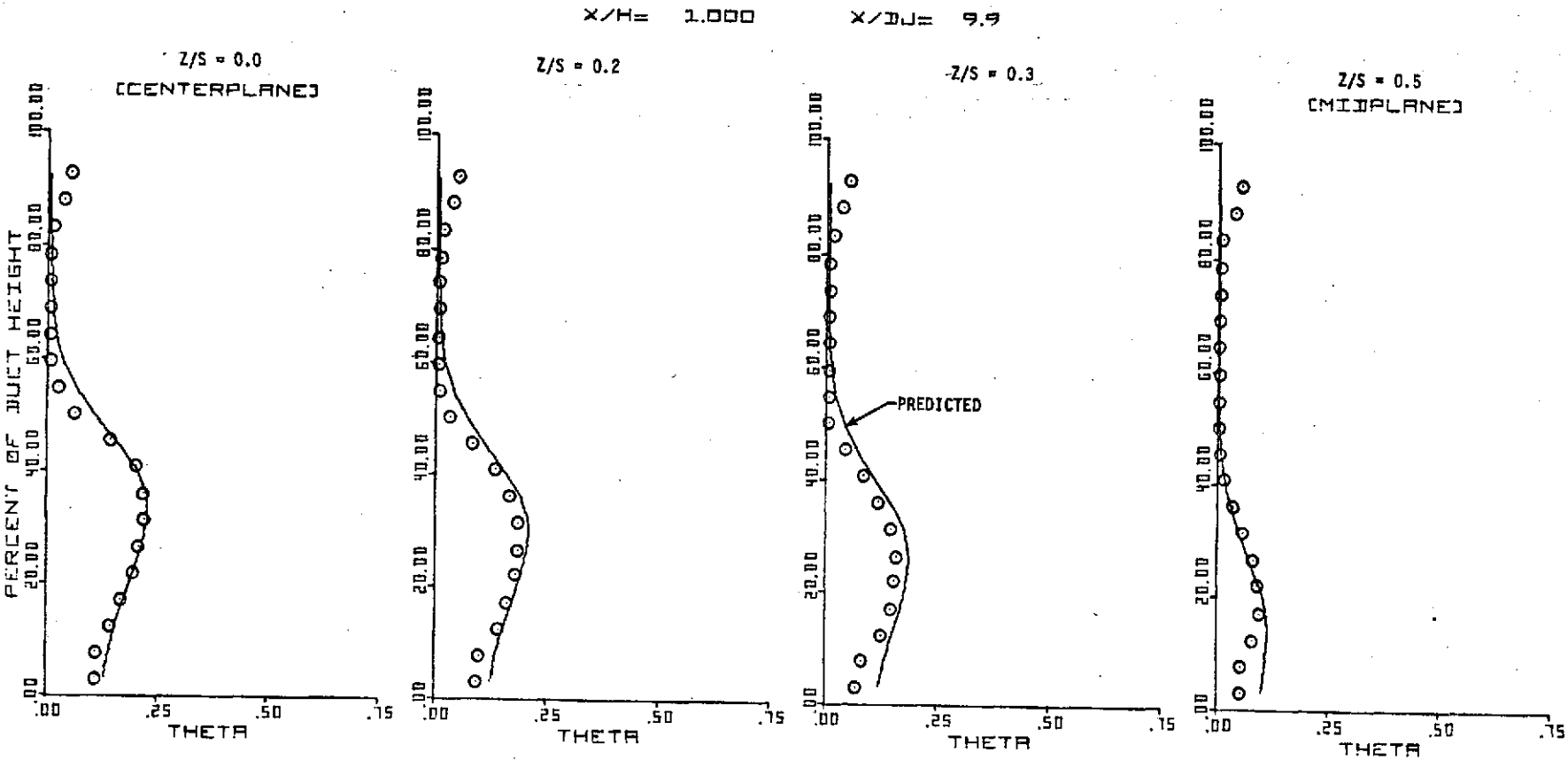

FIGURE 21. LATERAL PLANE TEMPERATURE PROFILE COMPARISONS
J - 6.3, S/D_J = 5.0, H/D_J = 9.9, X/H = 1.0

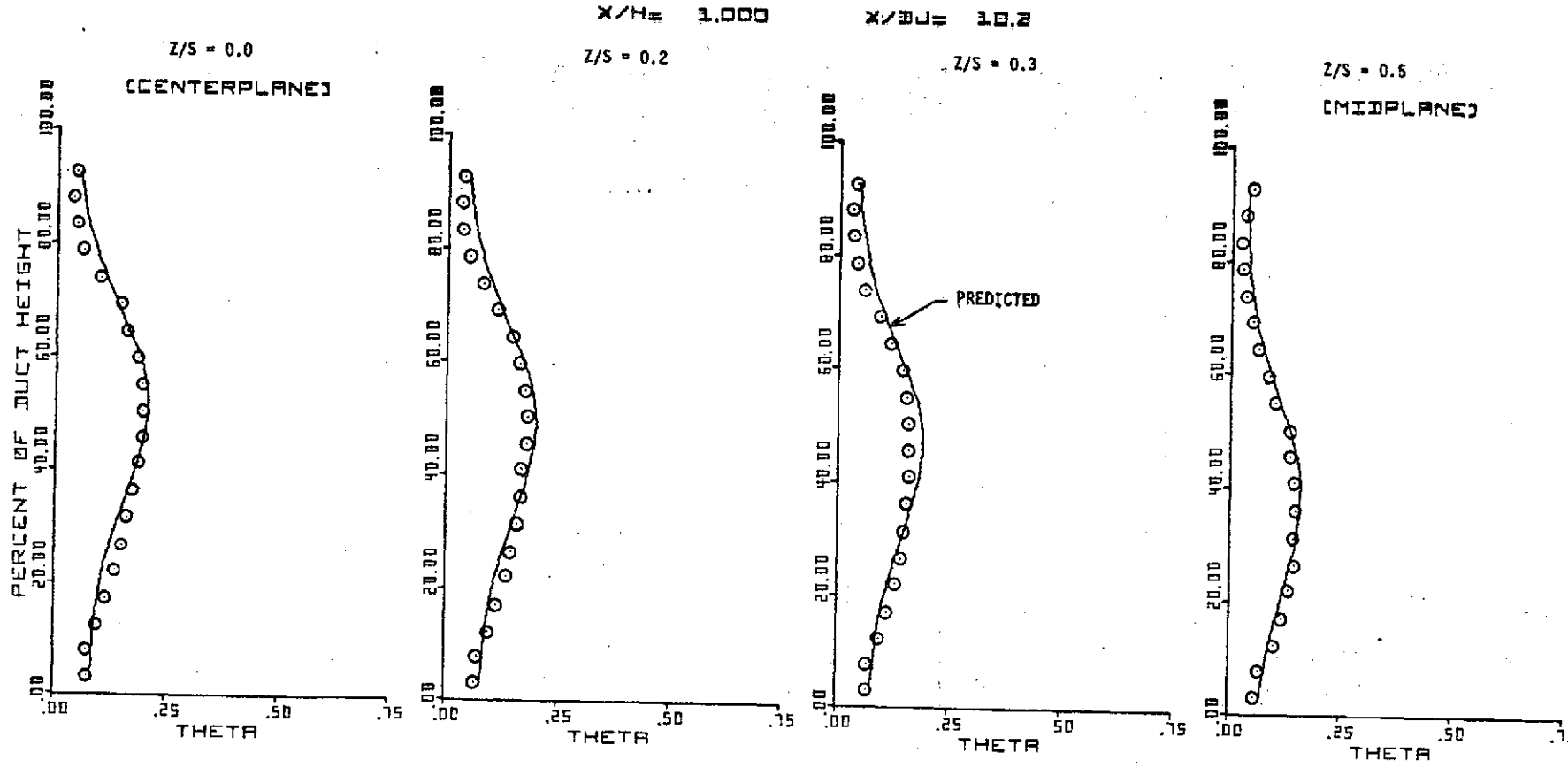

FIGURE 22. LATERAL PLANE TEMPERATURE PROFILE COMPARISONS
$J = 26.8$, $S/D_J = 5.1$, $H/D_J = 10.2$, $X/D = 1.0$

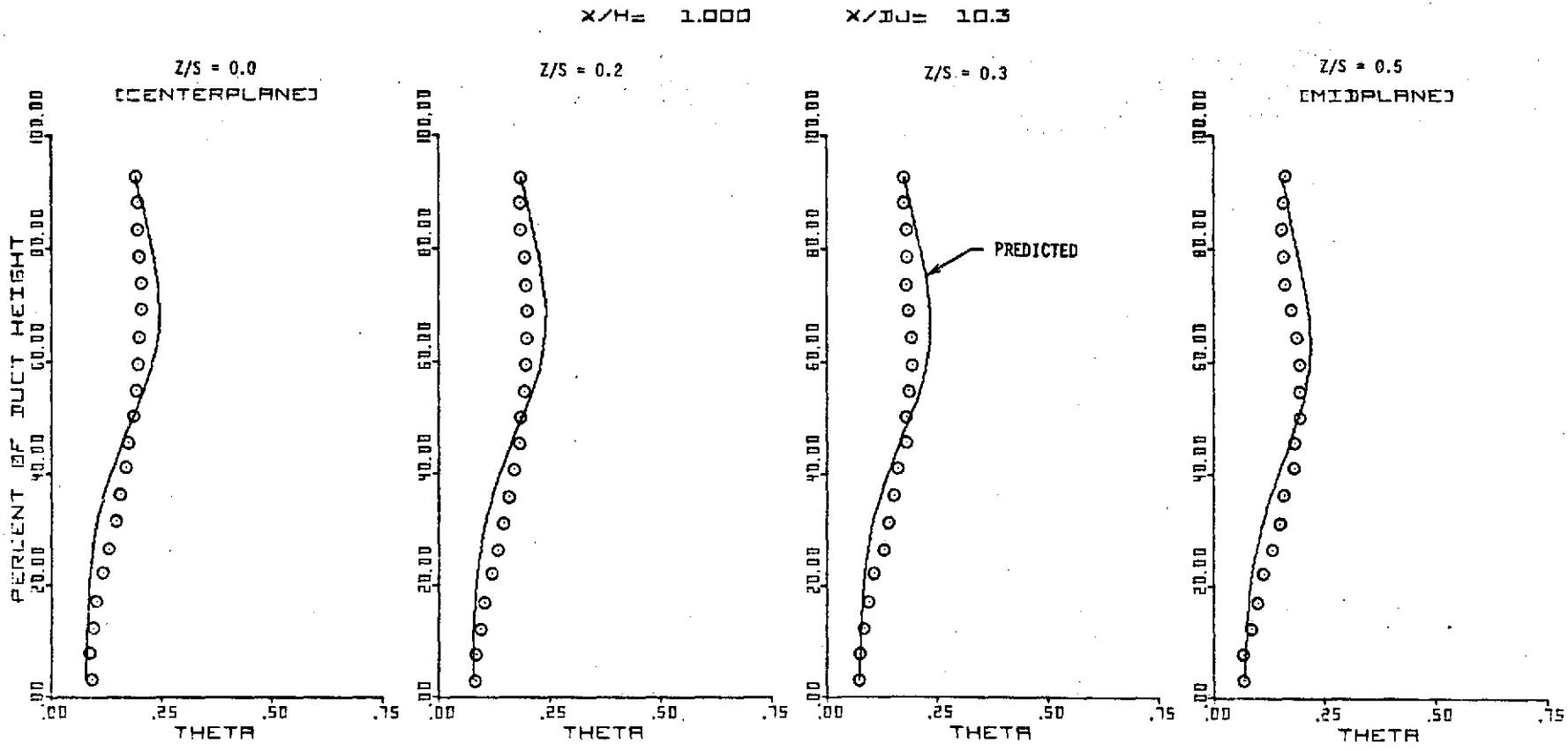

FIGURE 23. LATERAL PLANE TEMPERATURE PROFILE COMPARISONS
$J = 61.9$, $S/D_J = 5.1$, $H/D_J = 10.3$, $X/H = 1.0$

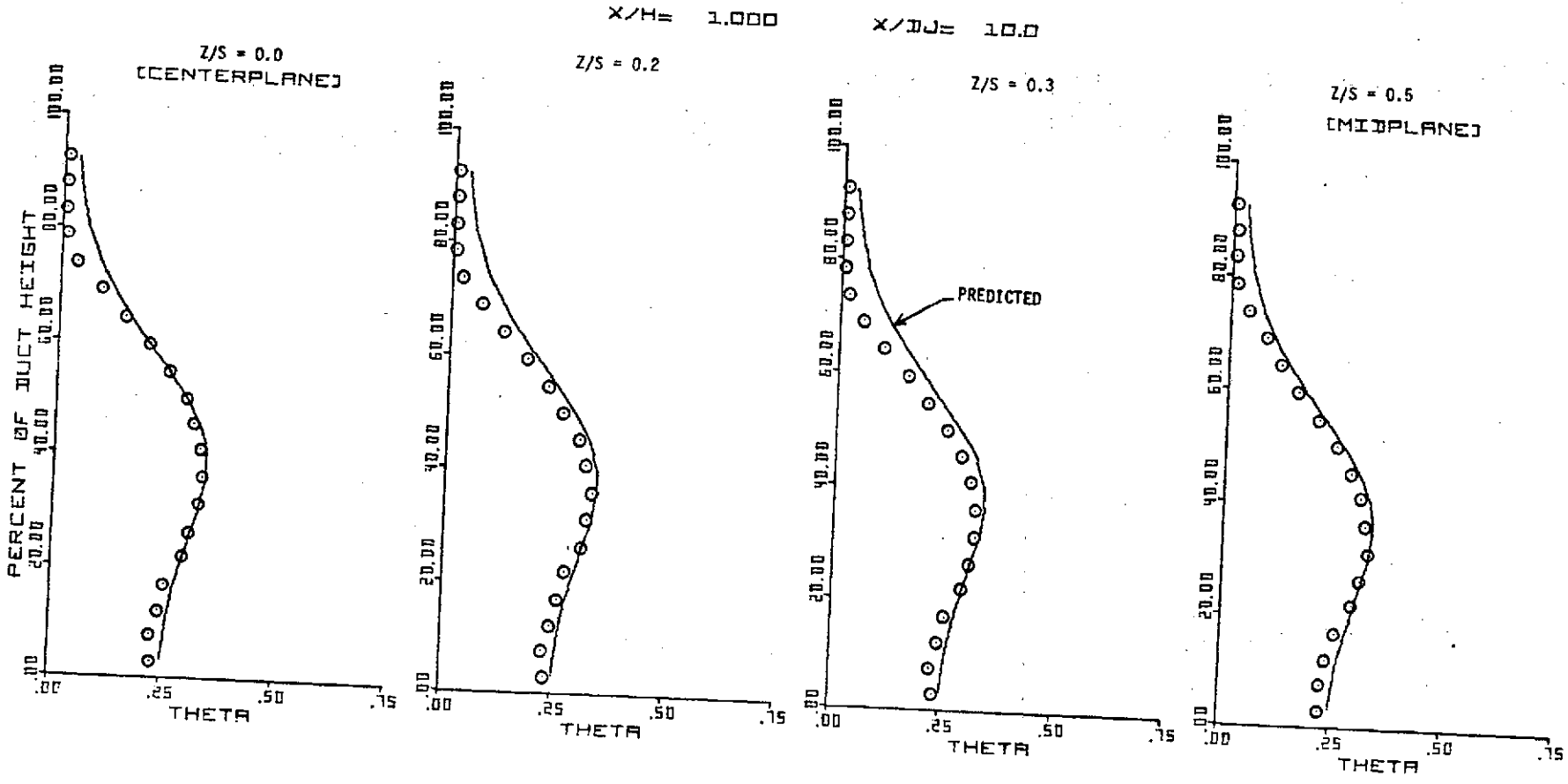

FIGURE 24. LATERAL PLANE TEMPERATURE PROFILE COMPARISONS
$J = 25.2$, $S/D_J = 2.5$, $H/D_J = 10.0$, $X/H = 1.0$

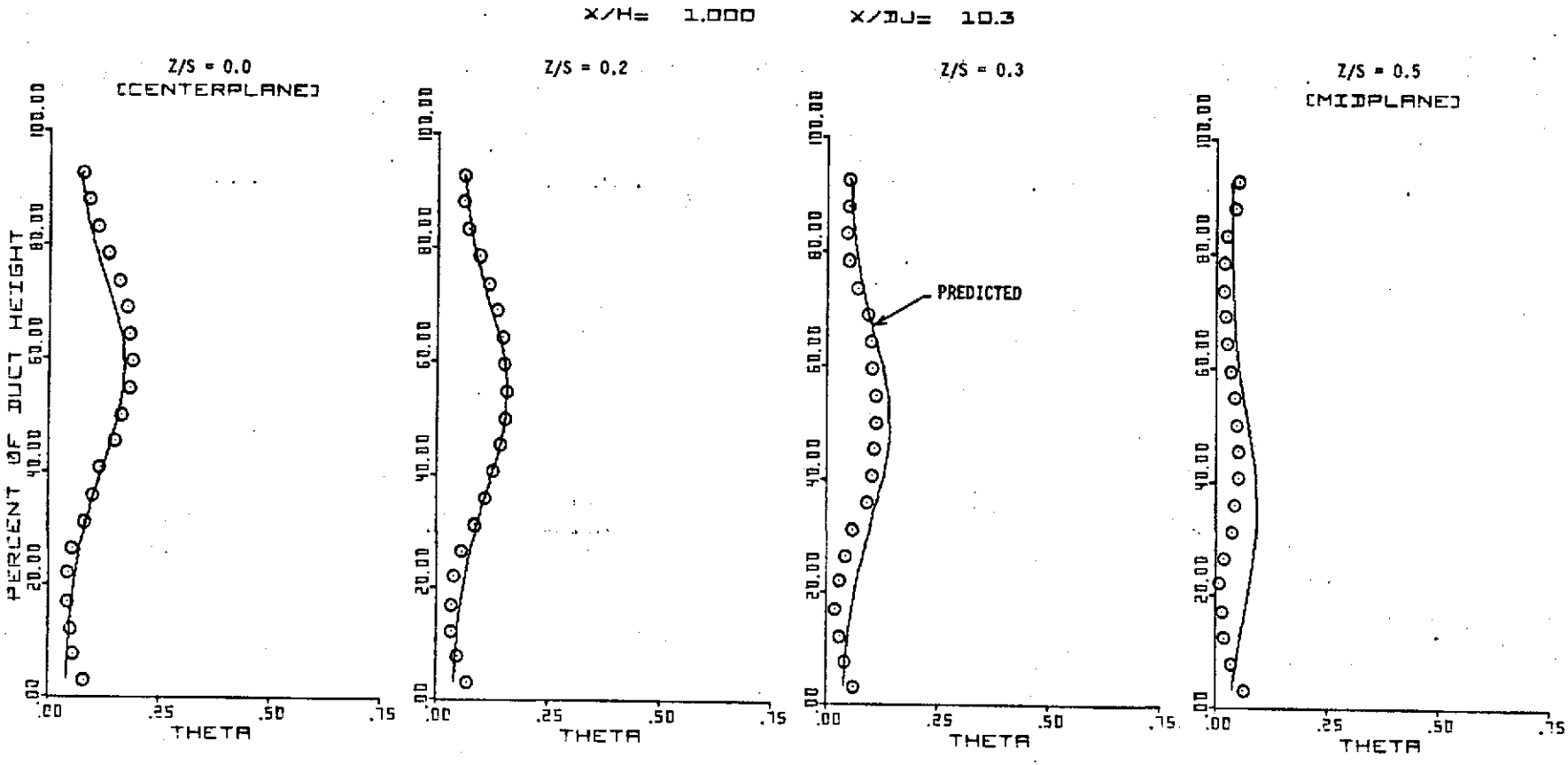

FIGURE 25. LATERAL PLANE TEMPERATURE PROFILE COMPARISONS
J = 27.6, S/D_J = 7.7, H/D_J = 10.3, X/H = 1.0

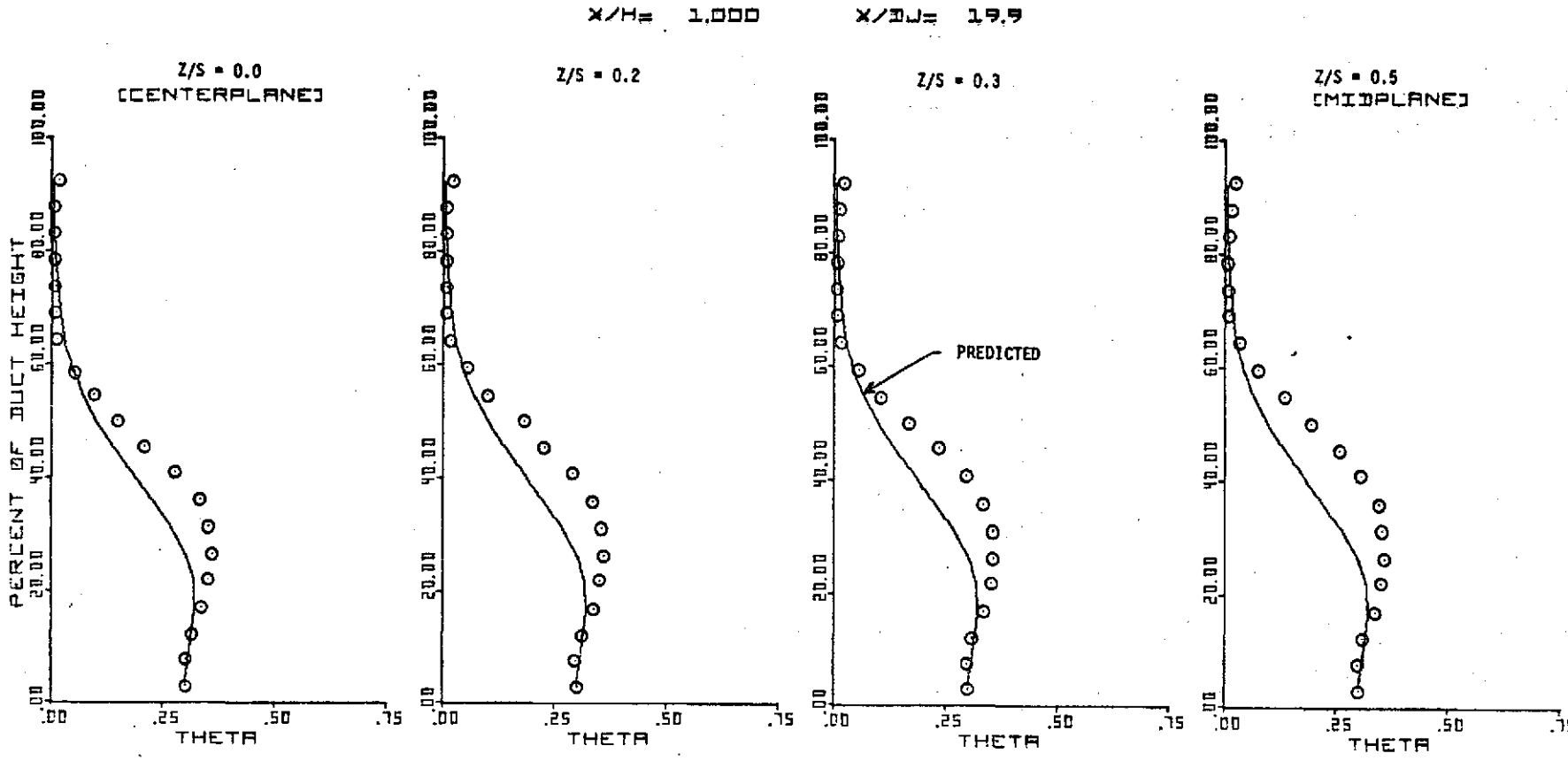

FIGURE 26. LATERAL PLANE TEMPERATURE PROFILE COMPARISONS
$J = 25$, $S/D_J = 2.5$, $H/D_J = 19.9$, $X/H = 1.0$

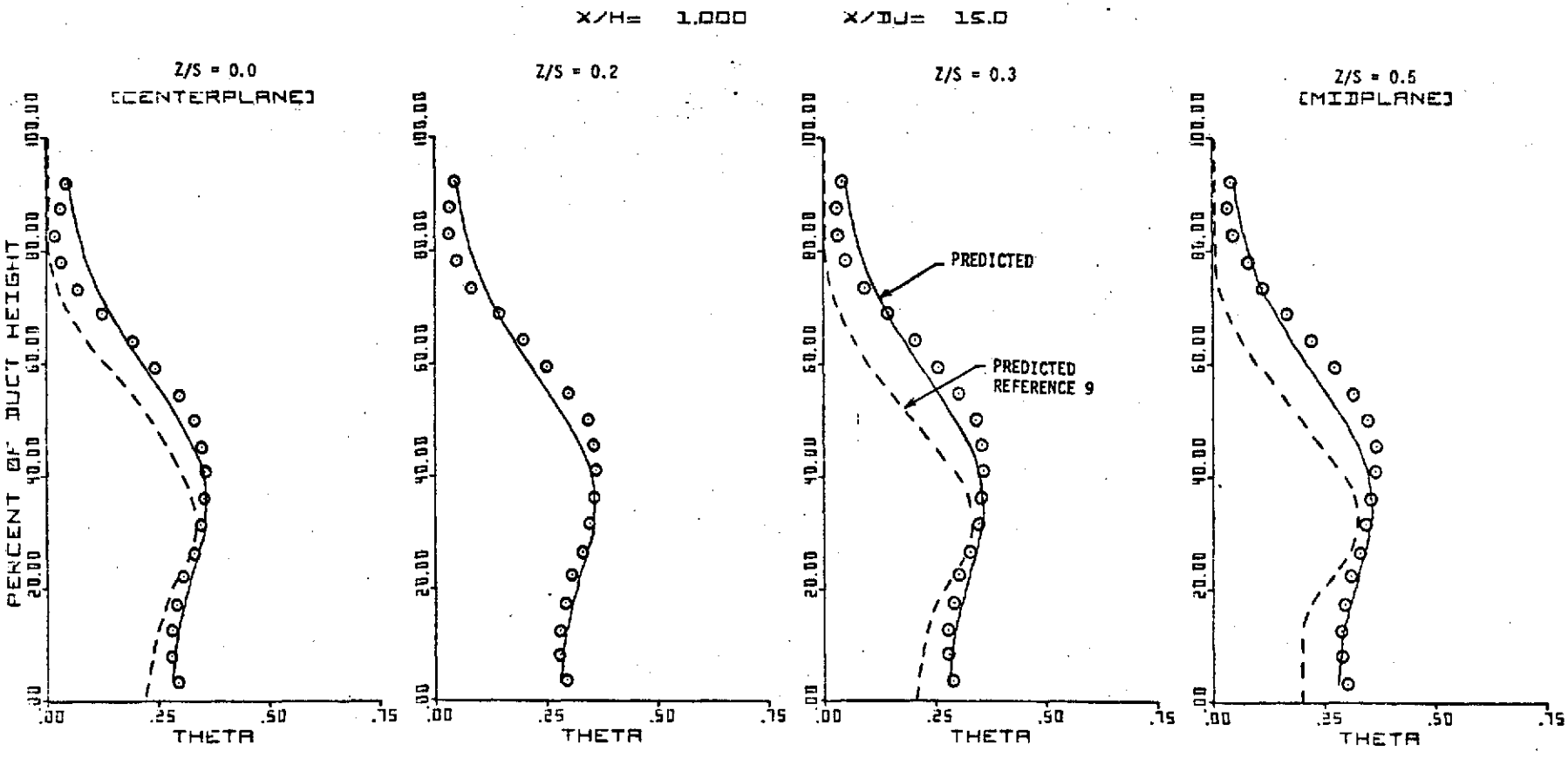

FIGURE 27. LATERAL PLANE TEMPERATURE PROFILE COMPARISONS
$J = 57.3$, $S/D_J = 2.5$, $H/D_J = 15$, $X/H = 1.0$

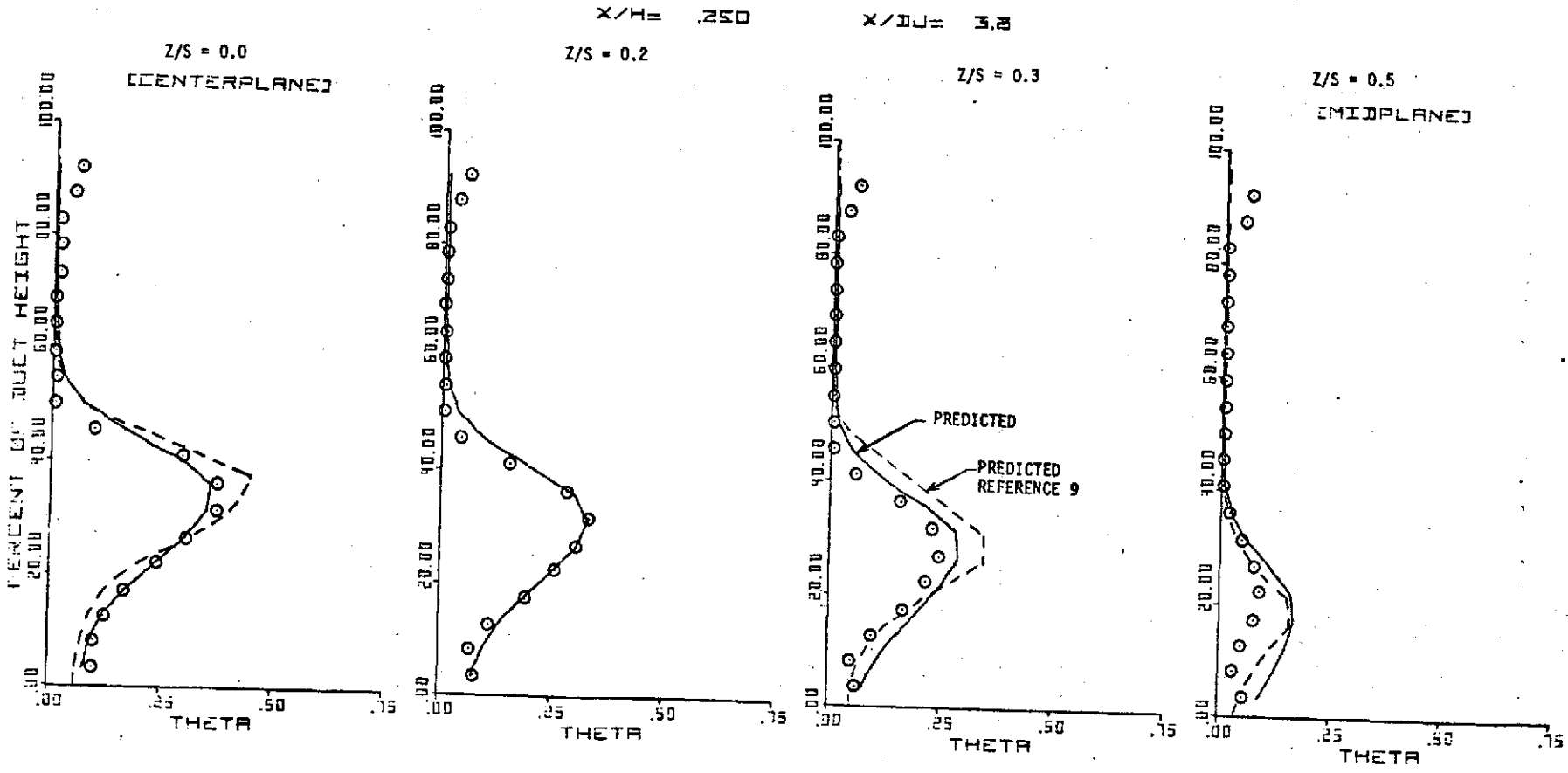

FIGURE 28. LATERAL PLANE TEMPERATURE PROFILE COMPARISONS
$J = 24.7$, $S/D_J = 5.0$, $H/D_J = 15$, $X/H = .25$

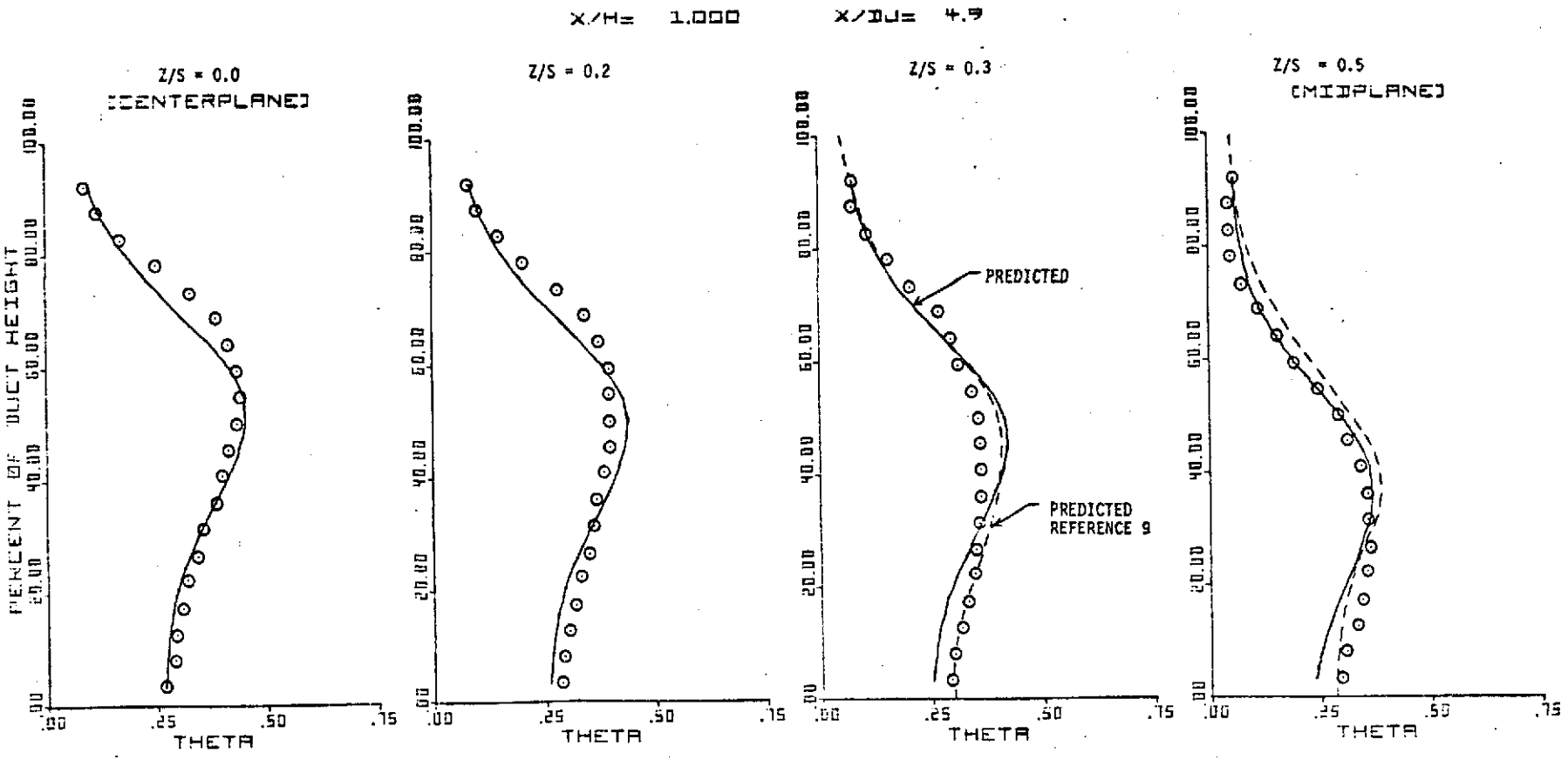

FIGURE 29. LATERAL PLANE TEMPERATURE PROFILE COMPARISONS
$J = 13.3$, $S/D_J = 2.5$, $H/D_J = 4.9$, $X/H = 1.0$

APPENDIX

TEMPERATURE FIELD PROGRAM

```
      C
      C     THIS PROGRAM WILL USE THE EQUATIONS DEVELOPED DURING THE MULTIPLE
      C     JET STUDY,NAS318026, TO DEFINE THE THERMAL FIELD DOWNSTREAM OF
      C     MULTIPLE JET INJECTION PORTS
      C
      C
            REAL NWIDTH
            COMMON / DIM / YC(10),YV(10),YH(20),XH(6),XDJ(10),ZS(6),
           *TICAP(10),TIMAX(10),HAFPOS(10),HAFNEG(10),PWIDTH(10),ET(10),
           *TWIDTH(10),NWIDTH(10),TZZ(6,21),YZZ(6,21),DEL(10),H,
           *THETA(10,21,20),XTHETA(10,21,20),TITLE(13),YD(20),YMID(20),TMID(20
           *),TBAR(10)
            COMMON / SINGLE / HD,RRHO,CD,RVEL,SDJ,RWDOT,HDJ,TIDEAL,XJ,SD,
           *RTEMP
            COMMON / RPLOT / XPLOT(22),YHPER(22),ITAB,NDSTRM,NOPLOT(6),YFIRST,
           *YDEL,XFIRST,XDEL
      C
            H=4.0
      C  ***AXIAL DIST., Y LOCATION, AND LATERPLT LOCATION ARRAYS ***
            DATA XH/.125,.250,.500,1.00,1.50,2.00/
            DATA YH/.034,.081,.127,.174,.221,.267,.314,.361,.408,.454,.501,
           *,548,.595,.641,.688,.735,.782,.828,.875,.922/
            DATA ZS/.0,.2,.4,.6,.8,1.0/
            NAMELIST/INPUT/HD,CD,XJ,SD,SH,RRHO,TIDEAL,RVEL,RTEMP,RWDOT,IPRNT
           *,ITAB,NDSTRM,NOPLOT,YFIRST,YDEL,XFIRST,XDEL,IPLOT
           1 FORMAT(13A6)
            READ(5,1)TITLE
            IF(CD.LT..01)CD=.62
            READ(5,INPUT,END=2000)
            WRITE(6,INPUT)
      C    *** CONVERT FROM X/H AND Y/H TO X/DJ AND Y/DJ
           2 FORMAT(1H1,13A6)
            DO 50 I=1,6
           50 XDJ(I)=XH(I)*HD/SQRT(CD)
            DO 60 I=1,20
           60 YD(I)=YH(I)*HD/SQRT(CD)
            IF(RWDOT.EQ.0.)WRITE(6,3)
            IF(RWDOT.EQ.0.)RWDOT=.20
            SDJ=SD/SQRT(CD)
            HDJ=HD/SQRT(CD)
            IF(RRHO.EQ.0.)RRHO=2.2
            IF(SH.EQ.0.)SH=SD/HD
            IF(TIDEAL.EQ.0.)TIDEAL=RWDOT
            DO 100 I=1,6
      C     *** ET EQUATION ***
            EN2=-.6816*(XDJ(I)**.44)*(SDJ**.44)*(HDJ**-1.0)*(XJ**.41)
            ET(I)=100.0*(1.0-EXP(EN2))
      C     *** CAP THETA AND MAX THETA EQUATIONS ***
            EXN=SQRT(SH/(1.+SH))
            TICAP(I)=(1.536*(XJ**-.4)*(XDJ(I)**-1.15))**(EXN)
            TIMAX(I)=TICAP(I)*(1.-TIDEAL)+TIDEAL
      C     *** PENETRATION EQUATIONS
      C     *** THERMAL ***
            YC(I)=.559*(XJ**.25)*(SDJ**.14)*(HDJ**.38)*(XDJ(I)**.17)
```

```
      EEX=EXP(-(XH(I)**2.0)*(1./SH-((XJ**.5)/3.5))/11.0)
      YC(I)=YC(I)*EEX
C
C  *** VELOCITY ***
      YV(I)=.549*(XJ**.12)*(SDJ**.23)*(HDJ**.57)*(XDJ(I)**.18)
C
C  *** PLUS AND MINUS SIDE HALF VALUES
C
      FX=.038*(XJ**1.62)*(XDJ(I)**1.1)*(HDJ***-3.67)*(SDJ**1.5)
      HAFPOS(I)=1.-0.5*EXP(-FX)
C
      FX=1.57*(XJ**-.3)*(SDJ***1.4)*(XDJ(I)**.9)
      HAFNEG(I)=1.-0.5*EXP(-FX)
C
C  *** HALF WIDTHS
C
      TWIDTH(I)=.3578*(XJ**.17)*(HDJ**.5)*(XDJ(I)**.3)
      PWIDTH(I)=.1623*(XJ**.18)*(HDJ**.5)*(XDJ(I)**.5)*(SDJ***-.25)
      NWIDTH(I)=TWIDTH(I)-PWIDTH(I)
      IF((YC(I)+PWIDTH(I)).GT.HDJ) PWIDTH(I)=HDJ-YC(I)
      IF((YC(I)-NWIDTH(I)).LT.0.) NWIDTH(I)=YC(I)
  100 CONTINUE
C
C  *** END OF CENTER PLANE PARAMETER CALCULATIONS
C
C   *** BEGIN OFF CENTERPLANE EVALUATIONS - DATA INDICATES THE RATIO
C       OF + AND - THETA HALF VALUES TO THETA MAX OFF CENTERPLANE IS
C       ESENTIALLY EUQAL TO THE CENTER PLANE RATIO,ALSO, THE OFF
C       CENTERPLANE HALFWIDTHS ARE EQUAL TO THE CENTERPLANE HALFWIDTHS
C
C
C
      DO 150 I=1,6
      FX=.4565*(XJ**.528)*(SDJ***-1.529)*(XDJ(I)**.828)
      YMID(I)=1.-EXP(-FX)
      FX=.227*(XJ**.67)*(SDJ***-1.0)*(XDJ(I)**.54)
  150 YMID(I)=1.-EXP(-FX)
C
C  *** CALCULATE OFF CENTERPLANE THETA AND Y MAX ***
      DO 200 I=1,6
      DO 200 K=1,6
      TZZ(I,K)=1.-(1.-TMID(I))*ZS(K)**2
  200 YZZ(I,K)=1.-(1.-YMID(I))*ZS(K)**2
C
C  *** NOW WILL ASSUME GAUSSIAN DISTRIBUTION TO GET FLOW FIELD ****
C       FIRST REPEAT THETA AND Y MAX VALUES FOR HALF SPAN FOUR TIMES
      DO 250 I=1,6
      N=0
      DO 210 K=7,11
      K1=5-N
      TZZ(I,K)=TZZ(I,K1)
      YZZ(I,K)=YZZ(I,K1)
  210 N=N+1
      N=2
      DO 220 K=12,16
      K1=N
      TZZ(I,K)=TZZ(I,K1)
```

```
112.            YZZ(I,K)=YZZ(I,K1)
113.          220 N=N+1
114.            N=0
115.            DO 230 K=17,21
116.            K1=5-N
117.            TZZ(I,K)=TZZ(I,K1)
118.            YZZ(I,K)=YZZ(I,K1)
119.          230 N=N+1
120.          250 CONTINUE
121.        C
122.        C
123.        C
124.        C
125.        C
126.            DO 500 M=1,6
127.            DO 500 K=1,21
128.            DO 500 I=1,20
129.            YMAX=YZZ(M,K)*YC(M)
130.            IF(YD(I).GE.YMAX) GO TO 400
131.            YI=YMAX-YD(I)
132.            TMIN=2.*HAFNEG(M)*T1MAX(M)-T1MAX(M)
133.            XEXP=EXP(-ALOG(2.)*(YI/NWIDTH(M))**2)
134.            THETA(M,K,I)=TZZ(M,K)*((T1MAX(M)-TMIN)*XEXP+TMIN)
135.            GO TO 500
136.          400 YI=YD(I)-YMAX
137.            TMIN=2.*HAFPOS(M)*T1MAX(M)-T1MAX(M)
138.            XEXP=EXP(-ALOG(2.)*(YI/PWIDTH(M))**2)
139.            THETA(M,K,I)=TZZ(M,K)*((T1MAX(M)-TMIN)*XEXP+TMIN)
140.          500 CONTINUE
141.        C
142.        C       THE FLOW FIELD HAS BEEN DEVELOPED OVER A TWO S SPAN FROM CENTER
143.        C       PLANE OF ORIFICE TO CENTER PLANE OF ORIFICE, NOW TRANSPOSE
144.        C       TO A FLOW FIELD THAT GOES FROM MIDPLANE TO MIDPLANE OVER 2S SPAN
145.        C
146.        C
147.        C
148.            DO 700 M=1,6
149.            DO 700 K=1,16
150.            DO 700 I=1,20
151.          700 XTHETA(M,K,I)=THETA(M,K+5,I)
152.            DO 720 M=1,6
153.            DO 720 K=17,21
154.            DO 720 I=1,20
155.          720 XTHETA(M,K,I)=THETA(M,K-15,I)
156.        C   *** GET AVERAGE THETA
157.            DO 750 M=1,6
158.            TBAR(M)=0.
159.            DO 750 K=1,21
160.            DO 750 I=1,20
161.          750 TBAR(M)=TBAR(M)+XTHETA(M,K,I)/20./21.
162.        C
163.        C       PATTERN FACTOR
164.        C
165.            DO 760 M=1,6
166.          760 DEL(M)=TBAR(M)/(1.-TBAR(M))
167.        C
168.            IF(IPRNT.EQ.0)CALL PRINT1
```

```
      2000 CONTINUE
         3 FORMAT(10X,'*** FLOW RATIO INPUT AS ZERO, SET EQUAL TO 0.20 ***')
C
C
C
C
      IF(IPLOT.EQ.0)CALL PLOT1
      END
```

END ELT, TIME: 0.4160 SECONDS.

```
      SUBROUTINE PLOT1
      REAL NWIDTH
      COMMON / DIM / YC(10),YV(10),YH(20),XH(6),XDJ(10),ZS(6),TICAP(10),
     *TIMAX(10),HAFPOS(10),HAFNEG(10),PWIDTH(10),ET(10),TWIDTH(10),
     *NWIDTH(10),TZZ(6,21),YZZ(6,21),DEL(10),H,THETA(10,21,20),
     *XTHETA(10,21,20),TITLE(13),YD(20),YMID(20),TMID(20),TBAR(10)
      COMMON / SINGLE / HD,RRHO,CD,RVEL,SDJ,RWDOT,HDJ,TIDEAL,XJ,SD,RTEMP
      COMMON / RPLOT / XPLOT(22),YHPER(22),ITAB,NDSTRM,NOPLOT(6),YFIRST,
     *YDEL,XFIRST,XDEL
      IF(NDSTRM.EQ.0)NDSTRM=4
      CALL PLOTS(0,0,7)
      CALL PLOT(7.,1.,0,-3)
C     *** (NM)= NUMBER OF POINT LOCATIONS IN DUCT HEIGHT ***
C     *** (NDSTRM)= DOWNSTREAM LOCATION OF LATERAL PLOTS ***
C     *** (NOPLOT)= DOWNSTREAM OR LATERAL LOCATIONS TO BE DELETED ***
      NM=20
      IF(ITAB.EQ.1)CALL SYMBOL(0,4,7,0,.20,'CENTERPLANE TEMPERATURE PROF
     *ILE COMPARISONS',0,,43)
      IF(ITAB.EQ.2)CALL SYMBOL(0,1,7,0,.20,'LATERAL PLANE TEMPERATURE PR
     *OFILE COMPARISONS',0,,45)
      CALL SYMBOL(3,8,6.5,.10,'J=',0,,2)
      CALL SYMBOL(5,7,6.5,.10,'S/DJ=',0,,5)
      CALL SYMBOL(8,1,6.5,.10,'H/DJ=',0,,5)
      CALL NUMBER(4,4,6.5,.10,XJ,0,,1)
      CALL NUMBER(6,7,6.5,.10,SDJ,0,,2)
      CALL NUMBER(9,1,6.5,.10,HDJ,0,,1)
      IF(ITAB.EQ.2)CALL SYMBOL(4,8,6,0,.10,'X/H=',0,,4)
      IF(ITAB.EQ.2)CALL SYMBOL(7,2,6.0,.10,'X/DJ=',0,,5)
      IF(ITAB.EQ.2)CALL NUMBER(5,7,6.0,.10,XH(NDSTRM),0,,3)
      IF(ITAB.EQ.2)CALL NUMBER(8,2,6.0,.10,XDJ(NDSTRM),0,,1)
      CALL AXIS(0,,0,,'PERCENT OF DUCT HEIGHT',22,5,,90,,YFIRST,YDELD
      YHPER(NM+1)=YFIRST
      YHPER(NM+2)=YDEL
      XPLOT(NM+1)=XFIRST
      XPLOT(NM+2)=XDEL
      MM=0
      NMD=1
   10 DO 15 M=1,6
      IF(NOPLOT(NMD).EQ.M)GO TO 15
      DO 13 I=1,20
      YHPER(I)=100.*YH(I)
      IF(ITAB.EQ.1)XPLOT(I)=XTHETA(M,6,I)
      IF(ITAB.EQ.2)XPLOT(I)=XTHETA(NDSTRM,M+5,I)
   13 CONTINUE
      IF(MM.EQ.0)GO TO 14
      CALL AXIS(0,,0,,'      ',5,5,,90,,YFIRST,YDEL)
   14 CALL AXIS(0,,0,,'THETA',-5,3,,0,,XFIRST,XDEL)
      MM=MM+1
      CALL LINE(XPLOT,YHPER,NM,1,0,1)
      IF(ITAB.EQ.1)CALL SYMBOL(0,7,5.5,.10,'X/DJ=',0,,5)
      IF(ITAB.EQ.1)CALL NUMBER(1.7,5.5,.10,XDJ(M),0,,1)
      IF(ITAB.EQ.1)CALL SYMBOL(0,7,5.2,.10,'X/H=',0,,4)
      IF(ITAB.EQ.1)CALL NUMBER(1.6,5.2,.10,XH(M),0,,3)
      IF(ITAB.EQ.2)CALL SYMBOL(0,8,5.5,.10,'ZZ/S=',0,,5)
```

```
      IF(ITAB.EQ.2)CALL NUMBER(1.8,5.5,.10,ZS(M),0.,1)
      IF(ITAB.EQ.2.AND.M.EQ.1)CALL SYMBOL(0.6,5.3,.10,'(CENTERPLANE)',0.
     *,13)
      IF(ITAB.EQ.2.AND.M.EQ.6)CALL SYMBOL(0.8,5.3,.10,'(MIDPLANE)',0.,10
     *)
      CALL PLOT(3.5,0.0,-3)
   15 IF(NOPLOT(NMD).EQ.M)NMD=NMD+1
      CALL PLOT(14.,-1.,999)
      RETURN
      END
```

END ELT, TIME: 0.1384 SECONDS.

PRINT1

```
      SUBROUTINE PRINT1
      REAL NWIDTH
      COMMON / DIM / YC(10),YV(10),YH(20),XH(6),XDJ(10),ZS(6),
     *TICAP(10), TIMAX(10), HAFPOS(10), HAFNEG(10), PWIDTH(10), ET(10),
     *TWIDTH(10),NWIDTH(10),TZZ(6,21),YZZ(6,21),DEL(10),H,
     *THETA(10,21,20),XTHETA(10,21,20),TITLE(13),YD(20),YMID(20),TMID(20
     *),TBAR(10)
      COMMON / SINGLE / HD,RRHO,CD,RVEL,SDJ,RWDOT,HDJ,TIDEAL,XJ,SD,
     *RTEMP
      DIMENSION ZZS(21),YS(20)
      HSI=H*2.54
      DATA ZZS/ 0.,.1,.2,.3,.4,.5,.6,.7,.8,.9,1.0,1.1,1.2,1.3,1.4,1.5,
     *1.6,1.7,1.8,1.9,2.0/
      WRITE(6,17)
      WRITE(6,16)TITLE
      WRITE(6,1)
      WRITE(6,2)XJ,SD
      WRITE(6,3)RTEMP,HD
      WRITE(6,4)RRHO,CD
      WRITE(6,5)RVEL,SDJ
      WRITE(6,6)RWDOT,HDJ
      WRITE(6,7)TIDEAL,HSI,H
      WRITE(6,8)
      WRITE(6,9)
      WRITE(6,20)
      DO 100 M=1,6
  100 WRITE(6,10)XH(M),XDJ(M),ET(M),TICAP(M),TIMAX(M),YC(M),YV(M),TBAR(M
     *),DEL(M)
      DO 110 I=1,20
  110 YS(I)=YH(I)*HD
      DO 500 M=1,6
      WRITE(6,11)
      WRITE(6,12)XH(M),XDJ(M)
      WRITE(6,13)(ZZS(K),K=1,11)
      WRITE(6,14)
      DO 150 I=1,20
  150 WRITE(6,15)YH(I),YD(I),YS(I),(XTHETA(M,K,I),K=1,11)
      WRITE(6,12)XH(M),XDJ(M)
      WRITE(6,13)(ZZS(K),K=11,21)
      WRITE(6,14)
      DO 160 I=1,20
  160 WRITE(6,15)YH(I),YD(I),YS(I),(XTHETA(M,K,I),K=11,21)
  500 CONTINUE
    1 FORMAT(///20X,'***** OPERATING CONDITIONS *****',T60,'**** DESIGN
     *CONDITIONS *****'//)
    2 FORMAT(20X,'MOMENTUM FLUX RATIO= ',F6.2,T60,'ORIFICE SPACING,S/D=
     * ',T90,F6.3)
    3 FORMAT(20X,'TEMPERATURE  RATIO = ',F6.2,T60,'ORIFICE SIZE, H/D =
     * ',T90,F6.3)
    4 FORMAT(20X,'DENSITY RATIO =      ',F6.2,T60,'ORIFICE DISCHARGE COE
     *F=',T90,F6.3)
    5 FORMAT(20X,'VELOCITY RATIO =     ',F6.2,T60,'EFFECTIVE SPACING,S/D
     *J=',T90,F6.3)
    6 FORMAT(20X,'FLOW RATE RATIO=     ',F6.2,T60,'EFFECTIVE ORIFICE SIZ
```

PRINT1

```
      *E,H/DJ= ',T90,F6.3)
    7 FORMAT(20X,'IDEAL THETA =         ',F6.2,T60,'DUCT HEIGHT= ',T90,
     *F6.3,' CM 'F6.3,' IN ')
    8 FORMAT(///40X,'****** MIXING AND CENTERPLANE DATA ******'///)
    9 FORMAT(13X,' DISTANCE',T27,'DISTANCE',T40,'MIXING EFF',T52,'CAP TH
     *ETA',T64,'MAX THETA',T76,'PENETRATION',T88,'PENETRATION',T100,'AVE
     * THETA',T112,'PATTERN')
   20 FORMAT(17X,'X/H',T30,'X/DJ',T45,'ET',T75,' X/DJ (TEMP)',T88,' X/D
     *J (VEL)',T113,'FACTOR')
   10 FORMAT(10X,9(2X,F10.4))
   11 FORMAT(1H1,T50,'*** TABLE OF THETA VALUES ***'//)
   12 FORMAT(1H0,T14,'X/H',F8.4,T30,'X/DJ',F8.4/)
   13 FORMAT(T4,'Z/S=',T20,11F10.4)
   14 FORMAT(T5,'Y/H',T11,'Y/DJ',T17,'Y/S')
   15 FORMAT(F5.3,F8.3,F6.3,T20,11F10.4)
   16 FORMAT(20X,'******   ',13A6,T110,'*******')
   17 FORMAT(1H1,//////20X,'********** AEROJET LIQUID ROCKET COMPANY MUL
     *TIPLE SET INJECTION FLOW FIELD PROGRAM   **********'///45X,'(DEVEL
     *OPED ON NASA LEWIS CONTRACT NAS 3-18026)'///)
C
      RETURN
      END
```

SAMPLE INPUT

```
$XQT FIELD
 $INPUT
 HD       =      .40000000E+01
 CD       =      .66130000E+00
 XJ       =      .13320000E+02
 SD       =      .20000000E+01
 SH       =      .50000000E+00
 RRHO     =      .22100000E+01
 TIDEAL   =      .27590000E+00
 RVEL     =      .24500000E+01
 RTEMP    =      .22100000E+01
 RWDOT    =      .35000000E+00
 IPRNT    =                +0
 ITAB     =                +1
 NDSTRM   =                +4
 NDPLOT   =                +1,          +5,          +0,          +0,
                           +0,          +0
 YFIRST   =      .00000000E+00
 YDEL     =      .20000000E+02
 XFIRST   =      .00000000E+00
 XDEL     =      .25000000E+00
 IPLOT    =                +0

 $END
```

DISTRIBUTION LIST FOR NASA CR-134795

NASA - Lewis Research Center
21000 Brookpark Road
Cleveland, OH 44135

	R. Lehan	MS 500-206	1
Attn:	Library	MS 60-3	2
	Technology Utilization	MS 3-19	1
	Report Control Office	MS 5-5	1
	Patent Counsel	MS 500-311	1
	Director of Aeronautics	MS 3-5	1
	Chief, Fluid Systems Components Division	MS 5-3	1
	Chief, V/STOL and Noise Division	MS 501-5	1
	Chief, Wind Tunnel & Flight Div	MS 86-1	1
	Chief, Airbreathing Engines Division	MS 60-4	1
	Chief, Physical Science Division	MS 301-1	1
	Head, Contract Section A Technology Procurement Br.	MS 500-206	1
	Lt. Col. G. J. Weden	MS 77-5	1
	Col. H. Staubs	MS 501-3	1
	W. T. Olson	MS 3-16	1
	J. F. Dugan, Jr.	MS 106-1	1
	R. A. Rudey	MS 60-6	1
	R. E. Jones	MS 60-6	1
	J. S. Grobman	MS 60-6	1
	E. A. Lezberg	MS 77-2	1
	D. J. Poferl	MS 77-2	1
	R. W. Graham	MS 301-1	1
	R. Siegel	MS 301-1	1
	J. D. Holdeman	MS 77-2	40
	G. J. VanFossen	MS 77-2	1
	R. S. Colladay	MS 77-2	1
	H. Davison	MS 77-2	1

II. OTHER GOVERNMENT AGENCIES — Number of Copies

NASA Scientific & Technical Information Facility
Attn: NASA Representative
P. O. Box 33
College Park, MD 20740
RQT 2448 — 10

NASA Headquarters
600 Independence Avenue S.W.
Washington, DC 20533
Attn: J. Suddreth (RLN) — 1

United States Army
Mr. Kent Smith, SAVDL/EU-TAT
Commanding Officer
Eustis Directorate - USA AMRDL
Fort Eustis, VA 23604 — 1

United States Army
Mr. Larry Bell
AVSCOM, AMSAV-EFP
Box 209
St. Louis, MO 63166 — 1

Air Force Office of Scientific Research
Mr. T. Wolfson
1400 Wilson Boulevard
Arlington, VA 22209 — 1

Defense Documentation Center (DDC)
Cameron Station
5010 Duke Street
Alexandria, VA 22314 — 1

NASA Langley Research Center
Langley Station
Hampton, VA 23365
Attn: Technical Library — 1
Dr. R. S. Levine, MS 213 — 1
Dr. D. Bushnell — 1

Environmental Protection Agency
Mr. Richard Munt
2565 Plymouth Road
Ann Arbor, ID 48105 — 1

II. OTHER GOVERNMENT AGENCIES

Naval Air Propulsion Test Center
Trenton, NJ 03628
Attn: Anthony Klarman 1
Bill Wagner 1

U.S. Department of Transportation
Attn: Anthony J. Broderick
Transportation Systems Center
Kendall Square
Cambridge, MA 02142 1

Wright Patterson Air Force Base
Attn: Dr. William S. Blazowski, AFAPL/SFF
Area B, Bldg. 18D
Dayton, OH 45433 1

Wright Patterson Air Force Base
Attn: Robert Henderson AFAPL/TBC
Area B, Bldg. 18D
Dayton, OH 45433 1

NASA Ames Research Center
Moffett Field, CA 94035
Attn: Library 1
Dr. I. G. Poppoff MS: 254-1 1

NASA Flight Research Center
Attn: Jack Nugent
Code R
P. O. Box 273
Edwards, CA 93523 1

Jet Propulsion Laboratory
4800 Oak Grove Drive
Pasadena, CA 91103
Attn: Jack H. Rupe MS: 125-224 1

Arnold Engineering Development Center
J. Division, Engine Test Facility
Arnold Air Force Station, TN 37389
Attn: Dr. C. E. Peters 1
Dr. P. T. Harsha 1
D. W. Male 1
Library 1

III. UNIVERSITIES

	Number of Copies
The Johns Hopkins University Attn: G. Dugger Applied Physics Laboratory 8621 Georgia Avenue Silver Springs, MD 20910	1
Stanford Research Institute Attn: F. E. Weil Menlo Park, CA 94025	1
Massachusetts Institute of Technology Attn: Prof. J. Heywood Department of Mechanical Engineering Cambridge, MA 02139	1
University of Cincinnati Attn: Prof. W. Kauffman Department of Aerospace Engineering Cincinnati, OH 45221	1
University of California Attn: Prof. R. F. Sawyer Department of Mechanical Engineering Berkeley, CA 94720	1
Purdue University School of Mechanical Engineering West Lafayette, IN 47907 Attn: Prof. A. M. Mellor Prof. V. W. Goldschmidt	1 1
Cornell University Attn: Prof. Sidney Liebovich Sibley School of Mechanical & Applied Engineering Upson & Grumman Halls Ithica, NY 14850	1
Northwestern University Attn: Prof. A. A. Kovitz Department of Mechanical Engineering & Astronautical Sciences Evenston, IL 60201	1
Virginia Polytechnic Institute & State University Attn: Prof. J. A. Shetz Department of Aerospace Engineering Blacksburg, VA 24061	1

III. UNIVERSITIES	Number of Copies
University of Illinois at Urbana - Champaign Attn: Prof. R. A. Strehlow Department of Aeronautical & Astronautical Engineering 101 Transportation Building Urbana, IL 61801	1
The University of Tennessee Space Institute Attn: Prof. G. W. Braun Tullahoma, TN 37388	1
Georgia Institute of Technology Attn: Prof. L. H. Bangert School of Aerospace Engineering Atlanta, GA 30332	1
Washington State University Attn: Dr. C. T. Crowe College of Engineering Research Division Pullman, WA 99163	1
University of Minnesota Attn: Prof. R. J. Goldstein Mechanical Engineering Department Minneapolis, MN 55455	1
Polytechnic Institute of Brooklyn Attn: Prof. P. M. Sforza Department of Aerospace Engineering and Applied Mechanics Long Island Graduate Center Route 110 Farmingdale, NY 11735	1
Michigan State University Attn: Prof. J. F. Foss Department of Mechanical Engineering 201 Engineering Building East Lansing, MI 48823	1
Case Western Reserve University Attn: Prof. I. Greber Dr. Y. Kamotani Division of Fluid, Thermal and Aerospace Sciences Cleveland, OH 44106	1 1

IV. CORPORATION		Number of Copies
United Aircraft Corporation		
Attn: R. Marshall		1
P. Goldberg		1
Library		1
Pratt & Whitney Aircraft Division		
400 Main Street		
East Hartford, CT 06108		
Detroit Diesel Allison Division		
Attn: Frank Verkamp		1
G. Tomlinson		1
Library		1
Department 8894, Plant 8		
P. O. Box 894		
Indianapolis, IN 46206		
Northern Research & Engineering Corp.		
Attn: E. R. Norster		
219 Vassar Street		
Cambridge, MA 02139		1
General Electric Company		
Attn: D. Bahr	H-33	1
Technical Information Center	N-32	1
Flight Propulsion Division		
Cincinnati, OH 45215		
General Electric Company		
Attn: Library Building		1
Dr. C. W. Smith,	2-40M	1
1000 Western Avenue		
West Lynn, MA 01905		
Curtiss-Wright Corporation		
Attn: S. Moskowitz		
One Passaic Street		
Woodridge, NJ 07075		1
AiResearch Manufacturing Company		
Attn: L. C. Wright		
2525 W. 190 Street		
Torrance, CA 90509		1

IV. CORPORATIONS

AVCO Corporation
Attn: Library 1
N. R. Marchionna 1
G. Opdyke 1
Lycoming Division
550 South Main Street
Stratford, CT 06497

Westinghouse Electric Corporation
Attn: Mr. Richard M. Chamberlin
Research and Development Center
Pittsburgh, PA 15235 1

International Harvester Company
Attn: W. A. Compton
Solar Division
2200 Pacific Highway
San Diego, CA 92112 1

Garrett/AiResearch Company
Attn: J. M. Haasis
402 South 36th Street
Phoenix, AZ 85034 1

Pratt & Whitney Aircraft
Attn: G. Lewis 1
G. B. Cox, Jr. 2
Florida Research & Development Center
Box 2691
West Palm Beach, FL 33402

Williams Research Corporation
Attn: Arnold Plumley
2280 W. Maple Road
Walled Lake, MI 48088 1

Aerospace Corporation
Attn: Owen W. Dykema
2350 East El Segundo Boulevard
El Segundo, CA 90061 1

Number of Copies

IV. CORPORATIONS

Advanced Technology Laboratories, Inc.
Attn: Dr. A. Ferri
Merrick and Stewart Avenues
Westbury, NY 11590 — 1

Bell Aerospace Company
Attn: Dr. S. W. Zelanzny
Advanced Technology Research
P. O. Box 1
Buffalo, NY 14240 — 1

Fluidyne Engineering Corporation
Attn: O. P. Lamb
5900 Olson Memorial Highway
Minneapolis, MN 55422 — 1

Surface Combustion Division
Attn: Dr. Klaus H. Hemsath
Midland-Ross Corporation
2375 Dorr Street
Toledo, OH 43691 — 1

General Motors Research Laboratories
Attn: Dr. G. Sovran
12 Mile and Mound Roads
Warren, MI 48090 — 1

Lockheed Missile and Space Company
Attn: Dr. R. J. Conti
Palo Alto Research Laboratory
3251 Hanover Street
Palo Alto, CA 94304 — 1